

2013-01-08

Corticospinal Tract Diffusion Tensor Imaging and Motor Function in Children following Perinatal Stroke

Hodge, Jacquelyn

Hodge, J. (2013). Corticospinal Tract Diffusion Tensor Imaging and Motor Function in Children following Perinatal Stroke (Master's thesis, University of Calgary, Calgary, Canada). Retrieved from <https://prism.ucalgary.ca>. doi:10.11575/PRISM/25473

<http://hdl.handle.net/11023/397>

Downloaded from PRISM Repository, University of Calgary

UNIVERSITY OF CALGARY

Corticospinal Tract Diffusion Tensor Imaging and Motor Function in Children following
Perinatal Stroke

by

Jacquelyn Hodge

A THESIS

SUBMITTED TO THE FACULTY OF GRADUATE STUDIES
IN PARTIAL FULFILMENT OF THE REQUIREMENTS FOR THE
DEGREE OF MASTER OF SCIENCE

DEPARTMENT OF NEUROSCIENCE

CALGARY, ALBERTA

JANUARY, 2013

© JACQUELYN HODGE 2013

Abstract

Perinatal stroke causes most hemiplegic cerebral palsy. Understanding developmental motor plasticity after perinatal injury is key to developing new therapies. Diffusion tensor imaging (DTI) facilitates this by interrogating functional white matter tracts (e.g. corticospinal tract, CST) but is not well studied in perinatal stroke. Our aim was to quantify CST integrity following perinatal stroke with DTI, evaluating different methodologies and correlations to motor outcome. Twenty-six children (Alberta Perinatal Stroke Project) underwent standardized DTI. Fiber tracking across different CST sections and ROI analysis compared CST diffusion variable (FA/AD/RD/MD) ratios (lesioned/non-lesioned). Correlations with validated motor outcome measures (AHA, MA, PSOM) were sought. DTI quantified differences in all CST diffusion parameters. Decreased FA and increased RD in the lesioned CST demonstrated the most robust correlations with motor outcomes. Analysis of defined CST subtracts may offer advantages over traditional DTI techniques. CST DTI carries both clinical and research utility in perinatal stroke.

Acknowledgements

I would like to thank my supervisor Dr. Adam Kirton and co-supervisor Dr. Brad Goodyear for all of their time, patience, and teaching. I would also like to thank my committee members; Drs. Ursula Tour and Shelagh Coutts and Dr. Deborah Dewey for acting as my external examiner. A special thank you to Drs. Christian Beaulieu, Helen Carlson and Min Liu for their time and expert help with this study; I wouldn't have known what I was doing without them and for all of the team involved with the Alberta Perinatal Stroke Program (APSP), thank you. Funding for this study was provided by the CIHR Training Program from the Alberta Children's Hospital Research Institute for Child and Maternal Health.

To all of my amazing family and friends who have supported me through the last few years.

Table of Contents

Abstract	ii
Acknowledgements	iii
Dedication	iv
Table of Contents	v
List of Tables	vii
List of Figures and Illustrations	viii
List of Symbols, Abbreviations and Nomenclature	xi
 CHAPTER 1 – BACKGROUND	 1
1. Perinatal Stroke and Statement of the Problem	1
1.1 Perinatal Stroke Syndromes	2
1.1.1 Symptomatic Neonatal Arterial Ischemic Stroke (NAIS)	3
1.1.2 Arterial Presumed Perinatal Ischemic Stroke (APPIS)	4
1.1.3 Periventricular Venous Infarction (PVI)	4
1.2 Outcome	6
1.2.1 Cerebral Palsy	6
1.3 CNS Motor Systems	7
1.3.1 Motor Cortex	7
1.3.2 Corticospinal Tract (CST)	8
1.4 Tools for Measuring Motor Outcome	12
1.4.1 Pediatric Stroke Outcome Measure (PSOM)	13
1.4.2 Assisting Hand Assessment (AHA)	13
1.4.3 Melbourne Assessment of Unilateral Upper Limb Function (MA)	14
1.5 Magnetic Resonance Imaging (MRI)	14
1.5.1 T1 Weighted and T2 Weighted MRI	16
1.6 MRI and Stroke	17
1.7 Diffusion Weighted Imaging (DWI) and Diffusion Tensor Imaging (DTI)	19
1.7.1 Cross-sectional Analysis (Region of Interest)	26
1.7.2 Track- based Analysis (Tractography)	26
1.8 DTI and Stroke	29
1.9 Aims and Hypotheses	33
 CHAPTER 2 - METHODS	 34
2. Patient Population	34
2.1.1. Motor Outcomes	35
2.1.2 Data Collection and Management	36
2.2 Image Acquisition	36
2.3 Image Analysis	36
2.3.1 DTIStudio Methods	37
2.3.2 Fiber Tracking Method	37
2.3.3 Quantification of Diffusion Variables within the Cerebral Peduncle	41
2.3.4 Quantification of the Ventral Midbrain Area at the Level of the Superior Midbrain	42
2.4 Statistical Analysis and Sample Size	43

2.4.1 Intra-rater Reliability	43
2.4.2 Distributions and Outliers.....	43
2.4.3 Primary Analysis	44
2.4.4 Correlation of Diffusion Variables with Motor Outcome	44
2.4.5 Sample Size Calculation.....	45
CHAPTER 3 – RESULTS	46
3. Population	46
3.1 Repeatability	51
3.2 Aim 1 –Quantify and Compare the Diffusion Parameters between the Lesioned and Non-lesioned CST in Children with Perinatal Stroke.....	52
3.2.1 Fractional Anisotropy (FA)	52
3.2.2 Axial Diffusivity (AD)	53
3.2.3 Radial Diffusivity (RD).....	54
3.2.4 Mean Diffusivity (MD)	55
3.3 Aim 2 – Compare Diffusion Parameters within Different Segments of the CST....	56
3.3.1 Fractional Anisotropy (FA)	56
3.3.2 Axial Diffusivity (AD)	57
3.3.3 Radial Diffusivity (RD).....	58
3.3.4 Mean Diffusivity (MD)	59
3.4 Mean Area Analysis of the Ventral Midbrain and Correlation with Motor Outcome	60
3.5 Aim 3 – Determine Associations between the CST Diffusion Measures and Motor Outcome.....	62
3.5.1 Diffusion Symmetry Associations with PSOM severity	62
3.5.2 Diffusion Symmetry Correlations with AHA and MA Motor Scores.....	66
3.6 Outliers, Normality, and Homogeneity of Variances	70
CHAPTER 4 – DISCUSSION.....	73
4. Comparison to Related Studies.....	73
4.1 Quantification of Diffusion Variables in the CST	74
4.2 The Non-lesioned CST	76
4.3 Fiber Tracking versus. Cross-sectional ROI Analysis.....	77
4.4 Correlation to Motor Outcome	78
4.5 Arterial versus. Venous Stroke	79
4.6 Future Directions: Modulating Developmental Plasticity	80
4.7 Limitations	81
4.8 Conclusions.....	82

List of Tables

Table 3.1. Patient demographics. Stroke types include middle cerebral artery (MCA) in the proximal M1 (PM1), distal M1 (DM1), posterior trunk (PT), or anterior trunk (AT), and periventricular infarction (PVI). PSOM score of 0 (normal), 0.5 (mild weakness with little impairment), 1 (moderate impairment), and 2 (severe impairment).	48
Table 3.2 Repeatability analysis for healthy and lesioned CST fiber counts in the full tract. Intraclass correlation (ICC) reported for 4 trials.....	51
Table 3.3. Repeatability analyses for healthy and lesioned CST mean FA in the full tract. Intraclass correlation (ICC) reported for 4 trials.....	52
Table 3.4. Correlation of diffusion variable SI for each tract with AHA and MA Motor Score. *Significant correlation.....	67
Table 3.5. Outliers were analysed and removed individually for each statistical test. Any outlier greater than 2 standard deviations from the mean was deemed extreme and removed.....	72

List of Figures and Illustrations

Figure 1.1. Perinatal stroke syndromes. Perinatal ischemic stroke can present in the acute period where diffusion weighted imaging confirms an acute neonatal arterial ischemic stroke (NAIS, left). Presumed perinatal ischemic strokes (PPIS) are fetal or neonatal injuries that present later in infancy, usually with congenital hemiplegia and remote infarction on MRI. Some are arterial infarcts (APPIS, middle) indistinguishable from chronic NAIS while others are periventricular venous infarction (PVI, right).....	3
Figure 1.2. Motor cortex and homunculus. Location of the motor cortex and associated motor areas (A) and the representative somatotopic motor map (homunculus) (B). Reprinted with permission from www.thebrain.mcgill.ca	8
Figure 1.3. The corticospinal tract trajectory. Starting in the motor cortex, pyramidal cells converge with fibers from the associated areas and travel ventrally down through the cerebral peduncles in the midbrain through the pons. The lateral CST fibers cross at the level of the decussation of the superior cerebellar peduncle, while the ventral CST remains ipsilateral until further down the spinal cord. Reprinted with permission from www.thebrain.mcgill.ca	11
Figure 1.4. (A) The spin of the hydrogen proton generates a small magnetic moment, μ . (B) Magnetic moments precess about the main magnetic field (B_0) at a nucleus specific frequency, ω , called the Larmor frequency (B).	16
Figure 1.5. (A) Example of a DWI showing restricted diffusion due to acute right MCA arterial stroke. (B) T1 MRI showing chronic perinatal stroke in the same arterial territory..	19
Figure 1.6. Illustration depicting diffusion within two different types of samples, one of which has similar molecular displacements in all directions (isotropic diffusion) the other having greater diffusion along one direction over another (anisotropic diffusion).	20
Figure 1.7. Schematic of how diffusion leads to reduced MR signal within an image voxel (represented as a square). (A) After an RF pulse is applied, all spins are in phase. (B) After application of a linear gradient in the x-direction, phase is altered as a function of x, due to the linear change in spin precessional frequency. (C) Over time, some spins diffuse (middle row) within, out of, or into the voxel. (D) After gradient reversal, spins along the middle row are not completely re-phased, due to their new x positions, leading to a reduced total voxel signal.	21
Figure 1.8. Diffusion Tensor Ellipsoid. The major eigenvalue, λ_1 , represents the direction with the greatest diffusion. λ_2 and λ_3 represent the minor eigenvalues and together they represent the water diffusion perpendicular to the major eigenvalue.	23
Figure 1.9. Illustration showing two types of FA images, grayscale (A) and color (B). Anterior-posterior is labelled green, the medial-lateral direction is red, and the superior-inferior direction is labelled blue.....	25

Figure 1.10. Fiber assignment by continuous tracking (FACT) method. Fiber tracking initiates within a ROI or seed voxel. Tract propagation follows the vector alignment of the ellipsoids.	27
Figure 2.1. Tractography Method. Locations of the ROIs on axial slices (A and C) and the mid-sagittal slice (B and D). The first ROI is drawn on the cerebral peduncle at the level of the decussation of the superior cerebellar peduncles (DSCP). From the tracking results, the posterior limb of the internal capsule is identified. Using the axial slice, the second ROI is selected and the CST is tracked.....	39
Figure 2.2. Tract segments used for analysis. An example image showing a lesioned CST full tract (yellow) and a healthy CST full tract (green). The tract segments are labelled: full (A), partial (B), upper (C), and mini (D).	41
Figure 2.3. ROI Analysis. Example of where the ROI was placed for diffusion analysis. ROI was $3 \times 3 \text{ mm}^2$	42
Figure 2.4. Ventral Midbrain Volume Method. The entire area of the cerebral peduncles was traced bilaterally. L represents the lesioned cerebral peduncle while NL represents the non-lesioned.	43
Figure 3.1. Example of lesioned and non-lesioned CST in a patient with a R. PVI. Healthy CST fibers (A), lesioned CST fibers (C), coronal view showing CST in both hemispheres (B) and lesion, and axial view (D).	49
Figure 3.2. Example of lesioned and non-lesioned CST in a patient with a L. MCA. Lesioned CST fibers (A), healthy CST fibers (B), coronal view showing CST in both hemispheres (C) and lesion, and axial view (D).	50
Figure 3.3. Mean FA values for lesioned versus non-lesioned CST across tract segments. n = 26 for full, 22 for upper, 23 for partial, 26 for mini, and 25 for ROI.	53
Figure 3.4. Mean AD values for lesioned versus non-lesioned CST across tract segments. n = 26 for full, 21 for upper, 23 for partial, 24 for mini, and 26 for ROI.	54
Figure 3.5. Mean RD values for lesioned versus non-lesioned CST across tract segments. n = 25 for full, 20 for upper, 23 for partial, 26 for mini, and 26 for ROI.	55
Figure 3.6. Mean MD values for lesioned versus non-lesioned CST across tract segments. n = 26 for full, 19 for upper, 23 for partial, 25 for mini, and 26 for ROI.	56
Figure 3.7. FA asymmetry across all tract segments. n = 26 in full, mini and ROI. n = 22 in upper and 23 for partial.	57
Figure 3.8. AD symmetry across all tract segments. n = 26 in full and ROI, n = 21 in upper, 23 in partial, and 24 in mini.	58

Figure 3.9. RD symmetry across all tract segments. n = 25 in full, 20 in upper, 23 in partial, 26 in mini and ROI.	59
Figure 3.10. MD symmetry across all tract segments. n = 26 in full and ROI, 19 in upper, 23 in partial, and 25 in mini.	60
Figure 3.11. Ventral midbrain mean area calculations of the lesioned and non-lesioned CST. n = 26.	61
Figure 3.12. Ventral midbrain mean area symmetry across severe (PSOM = 2) and non-severe motor outcome (PSOM = 0-1), n = 26. * p < 0.05.	61
Figure 3.13. The relationship between motor assessment score (AHA and MA) and ventral midbrain area symmetry, n = 16.	62
Figure 3.14. Full tract diffusion variables across severe and non-severe motor outcome, n = 24 in FA, 26 in AD, and 25 in RD and MD.	63
Figure 3.15. Partial tract diffusion variable symmetries across severe and non-severe motor outcome, n = 26 in FA and RD and 25 in AD and MD.	64
Figure 3.16. Upper tract diffusion variable symmetries across severe and non-severe motor outcome, n = 22 in FA, 20 in AD, RD, and MD.	64
Figure 3.17. Mini tract diffusion variable symmetries across severe and non-severe motor outcome, n = 26 in FA, RD and MD, and 25 in AD.	65
Figure 3.18. Cross-section ROI analysis diffusion variable symmetries across severe and non-severe motor outcome.	66
Figure 3.19. The relationship between motor assessment score (AHA and MA) and inter-hemispheric symmetry of CST diffusion in the upper tract, n = 16.	68
Figure 3.20. The relationship between motor assessment score (AHA and MA) and inter-hemispheric symmetry of CST diffusion in the full tract, n = 16.	68
Figure 3.21. The relationship between motor assessment score (AHA and MA) and inter-hemispheric symmetry of CST diffusion in the partial tract, n = 16.	69
Figure 3.22. The relationship between motor assessment score (AHA and MA) and inter-hemispheric symmetry of CST diffusion in the mini tract, n = 16.	69
Figure 3.23. The relationship between motor assessment score (AHA and MA) and inter-hemispheric symmetry of CST diffusion in the cross section ROI analysis, n = 16.	70

List of Symbols, Abbreviations and Nomenclature

Symbol	Definition
ACH	Alberta Children's Hospital
AD	Axial diffusivity
ADC	Apparent diffusion coefficient
AHA	Assisting hand assessment
APPIS	Arterial presumed perinatal ischemic stroke
APSP	Alberta perinatal stroke program
AT	Anterior trunk
CP	Cerebral palsy
CST	Corticospinal tract
DM1	Distal M1
DSCP	Decussation of the superior cerebellar peduncle
DTI	Diffusion tensor imaging
DWI	Diffusion weighted imaging
FA	Fractional anisotropy
FACT	Fiber assignment by continuous tracking
FT	Full tract
ICD	International classification of disease codes
ICF	International classification of functioning, disability, and health
MA	Melbourne assessment of unilateral upper limb function
MCA	Middle cerebral artery
MD	Mean diffusivity
MRI	Magnetic resonance imaging
MT	Mini tract
NAIS	Neonatal arterial ischemic stroke
PLIC	Posterior limb of the internal capsule
PM1	Proximal M1
PPIS	Presumed perinatal ischemic stroke
PSOM	Pediatric stroke outcome scale
PT	Posterior trunk
PT	Partial tract
PVI	Periventricular venous infarction
PVL	Periventricular leukomalacia
RD	Radial diffusivity
RF	Radio frequency
ROI	Region of interest
rTMS	Repetitive transcranial magnetic stimulation
SD	Standard deviation
SI	Symmetry index
T	Tesla
TMS	Transcranial magnetic stimulation
UT	Upper tract
ω	Larmor frequency

CHAPTER 1 – BACKGROUND

1. Perinatal Stroke and Statement of the Problem

Blockage of blood flow deprives brain tissue of nutrients, oxygen, and glucose essential for survival, resulting in a focal infarction (e.g., an ischemic stroke) and permanent damage. The perinatal timeframe is the most focused period of risk for ischemic stroke during the lifespan. With the current estimated incidence of at least 1:3500 live births¹, ischemic stroke is one of the most common causes of neurological disease in children and the leading cause of hemiplegic cerebral palsy (CP)^{2,3}. Perinatal stroke is defined as “a group of heterogeneous disorders in which there is a focal disruption of cerebral blood flow secondary to arterial or venous thrombosis or embolization, between 20 weeks of fetal life through to the 28th postnatal day, and confirmed by neuroimaging or neuropathological studies”⁴.

Neuroimaging, in particular magnetic resonance imaging (MRI), has emerged as a valuable clinical tool in the diagnosis of perinatal stroke^{5,6}. Diffusion tensor imaging (DTI), a type of imaging that measures how water moves within the brain, allows for visualization of white matter tracts. This imaging technique holds promise for determining at the microscopic level how specific connections are affected after perinatal stroke with the added possibility of outcome prediction. However, appropriate methodologies and clinical utility have yet to be determined. It is the goal of this thesis to develop and test DTI measures of corticospinal tract integrity and their relationship to motor outcome.

In this first chapter we will describe perinatal stroke and review MRI and DTI, with focus on the methods used in this thesis. Chapter 2 describes the methodology of the main study in

detail and Chapter 3 presents our findings. The final Chapter 4 will discuss the significance of our findings, how it relates to the current literature, and offer suggestions for future work.

1.1 Perinatal Stroke Syndromes

There are several forms of ischemic perinatal stroke syndromes that will be defined below and are the focus of this thesis. Other forms of perinatal stroke such as neonatal cerebral sinovenous thrombosis (CSVT), neonatal hemorrhagic stroke, and preterm vascular injuries (e.g., intraventricular haemorrhage) are not discussed here.

Recent advances in neuroimaging have improved recognition and classification of different ischemic stroke types in the fetus and newborn^{6,7}. Now classified based on the mechanism and timing of injury and presentation, three stroke syndromes currently predominate (Figure 1.1): neonatal arterial ischemic stroke (NAIS), which occurs during the newborn period; arterial presumed perinatal ischemic stroke (APPIS), likely occurring at the same time but diagnosed later in infancy when congenital hemiparesis is recognized; and the more recently defined periventricular venous infarction (PVI)⁶, which has a distinct antenatal timing and mechanism.

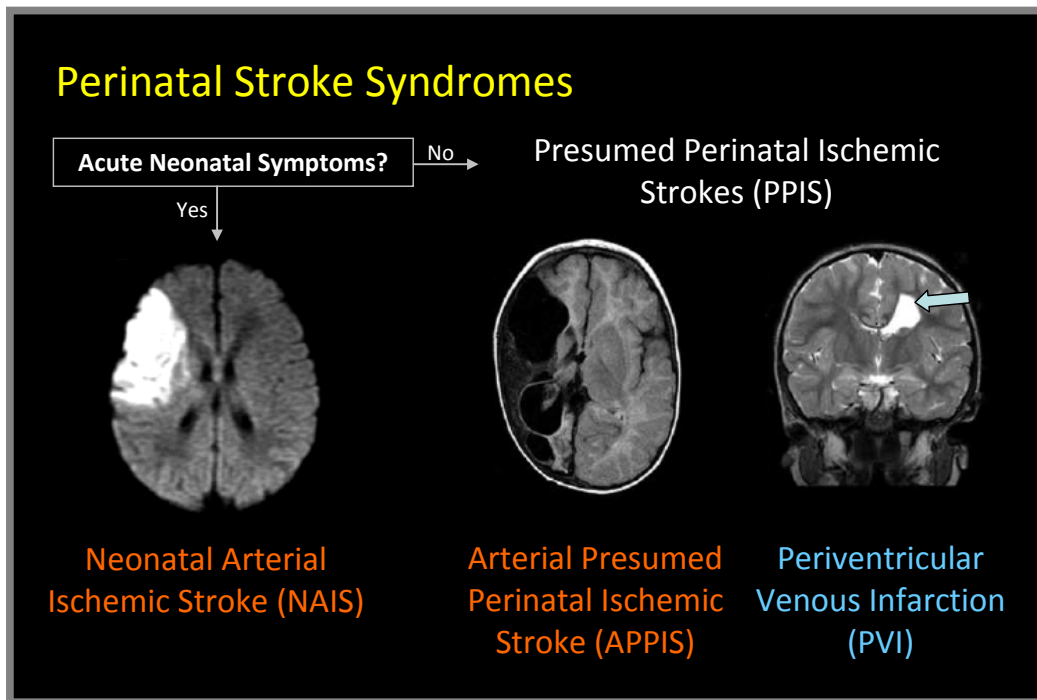


Figure 1.1. Perinatal stroke syndromes. Perinatal ischemic stroke can present in the acute period where diffusion weighted imaging confirms an acute neonatal arterial ischemic stroke (NAIS, left). Presumed perinatal ischemic strokes (PPIS) are fetal or neonatal injuries that present later in infancy, usually with congenital hemiplegia and remote infarction on MRI. Some are arterial infarcts (APPIS, middle) indistinguishable from chronic NAIS while others are periventricular venous infarction (PVI, right).

1.1.1 Symptomatic Neonatal Arterial Ischemic Stroke (NAIS)

As the name suggests, the NAIS syndrome presents with acute symptoms (often seizures) during the newborn period. In these cases, diffusion MRI reveals acute arterial infarctions. Surprisingly, these neonates present clinically as unremarkable, and therefore are often not recognized acutely. Due to the relatively simple diagnosis of NAIS, it allows for the evaluation of potentially causative factors, and thus accounts for more than 90% of the published literature⁸. Despite, representing less than 50% of cases, most perinatal stroke studies to date are limited to NAIS.

1.1.2 Arterial Presumed Perinatal Ischemic Stroke (APPIS)

On the other hand, many neonates with acute arterial ischemic stroke do not exhibit any symptoms during the neonatal period, but rather present with their deficits at around 4 -6 months of life. Such presumed perinatal ischemic stroke (PPIS) defines a child with normal perinatal history, who presents with neurological morbidity (usually hemiparesis) later in infancy⁹⁻¹¹ due to remote focal infarction, as revealed by imaging^{4,6}. Present imaging-based studies suggest arterial PPIS (APPIS) may be the most common but least-studied of the perinatal stroke syndromes^{4,12,13}. Like NAIS, APPIS most often results from middle cerebral artery occlusion^{10,14-16}. Previous research suggests that these two syndromes may represent the same disease, and merely differ in their time of presentation^{6,17}.

1.1.3 Periventricular Venous Infarction (PVI)

Conversely, PVI occurs secondary to a germinal matrix haemorrhage *in utero* prior to 34 weeks of gestation. Over 13, 000 delivered premature babies are affected by germinal matrix haemorrhages (GMH) annually in North America¹⁸ but the term-born equivalent of PVI is only more recently being recognized. GMH occurs and then blocks the medullary veins, which drain in the periventricular white matter. This results in a venous infarction, often causing damage to the corticospinal tract (CST) and leading to hemiplegic cerebral palsy^{19,20}. This same process is increasingly described as occurring *inutero*^{21,22} with term born infants presenting as PPIS^{23,24}. Modern MRI has allowed for the detection of remote germinal matrix bleeds, permitting accurate retrospective diagnosis of PVI^{6,17,23}. Retrospective analysis of early CP imaging studies suggest

PVI in 35-55% of cases²⁵⁻²⁹, and a recent study characterized PVI as the second most common variety of PPIS⁶.

This imaging-based classification system has been validated by a number of studies that have demonstrated its effectiveness in the prediction of neurological outcomes^{6,30}, recognition of novel risk factors^{17,31,32}, imaging markers of disease processes,^{5,33,34} and new targets for therapeutic interventions³⁵. Many cases of NAIS and APPIS appear to differ only in their timing of presentation with otherwise indistinguishable patterns of arterial infarction on neuroimaging. It is therefore likely that NAIS and APPIS often represent the same disease¹⁷. While the mechanisms differ between arterial and venous perinatal strokes, they share similar long-term motor outcomes.

The pathophysiology of perinatal stroke continues to be poorly understood. What causes the majority of perinatal strokes remains unknown despite the increasing case-control and large-scale studies^{2,8,17}. Recent work suggests acute perinatal clinical factors and some prothrombotic markers differ between syndromes,¹⁷ but more detailed investigation is required to clarify true pathophysiology. Possible risk factors for perinatal stroke are diverse and include: complex congenital heart disease, prothrombotic conditions, placental disease, perinatal infections, maternal and obstetrical factors among others². Risk factors presenting definitive causal evidence such as meningitis and complex heart disease make up < 20% of NAIS cases. Most studies to date that have investigated causality of stroke in the perinatal period have focused on NAIS while the possible mechanisms for APPIS and PVI are largely unknown. Without knowledge of the causes, effective treatments and preventative strategies will not likely be realized anytime soon, if ever. Therefore, the burden of perinatal stroke and hemiplegic CP will likely persist, leaving the need for better understanding of motor recovery and developmental plasticity.

1.2 Outcome

Most children who survive perinatal stroke suffer neurological impairments including intellectual disabilities, language disorders, developmental and behavioural problems, and epilepsy^{1,36}. More than 70% of all perinatal stroke survivors face lifelong neuro-developmental deficits^{3,10}. Children with perinatal stroke have lifelong morbidity, amplifying the burden on the child, their families, and society³⁷. Motor disability is the most consistent adverse outcome across all perinatal stroke types and likely has the largest impact on overall quality of life.

1.2.1 Cerebral Palsy

The most common neurological deficit that plagues this population is chronic motor weakness. Loss or impairment of motor function that results in physical disability secondary to early brain injury is collectively referred to as CP. CP is caused when there is damage to the motor areas of the developing brain; it affects muscles and the ability to control them. This can lead to difficulty with muscle tone, muscle control, coordination, reflexes, balance, and posture. CP is a broad encompassing definition for congenital motor dysfunction and can be categorized into subtypes based on severity, topographical distribution, or motor function. Traditional topographical distribution classifications include: monoplegia when one limb is affected; diplegia with bilateral leg motor impairment, often associated with premature brain injury such as periventricular leukomalacia (PVL); triplegia when three limbs are affected; quadriplegia, referring to all four limbs and associated with many different bilateral and diffuse brain injuries; and dyskinetic often associated with deep grey matter injuries such as acute total hypoxic-ischemic encephalopathy. These are just a few examples of many. When one side of the body is affected, it is referred to as hemiplegic CP, or more accurately hemiparetic CP (e.g., weakness (paresis) without a complete

lack of movement (plegia)). Hemiparetic CP accounts for > 30-40% of term born CP cases with perinatal stroke accounting for the vast majority of cases^{3,10}.

1.3 CNS Motor Systems

Motor weakness in CP, and in particular perinatal stroke, is often the direct result of damage to one or more of the major components of the motor system. While motor control is complex, two basic components have been identified that may be the site of primary injury in perinatal stroke resulting in hemiparetic CP: the motor cortex and CST. For the purposes of this thesis an oversimplified description ignoring the many complex areas involved in motor control (like the basal ganglia and cerebellum) will focus on such a two-component model.

1.3.1 Motor Cortex

Voluntary movement originates primarily from the motor cortex with the prefrontal and anterior parietal cortex also playing a role. Divided into two main areas, the primary motor cortex (area 4 or M1) is centered along the anterior bank of the precentral gyrus of the frontal lobe (Figure 1.2A) and area 6, which lies rostral to the primary motor cortex and is further divided into the pre-motor cortex (guides body movements by integrating sensory information) and supplementary motor cortex (planning complex movements and coordination of movements involving both hands) (Figure 1.2A). Like most brain functions, movement is controlled predominantly by the contralateral hemisphere. All of these areas are intimately networked and connect with the homologous areas of the opposite hemisphere. The primary motor cortex and somatosensory cortex have comparable somatotopic organization (maps reproducing the human body on a small scale) with area devoted to each body part directly proportional to the

complexity of sensorimotor functions they perform. Motor control is topographically arranged according to the motor maps (homunculus) with the upper extremity placed between the lower (medially) and faces (laterally) (Figure 1.2B).

Large pyramidal neurons from layer 5 of the motor cortex converge with fibers from the pre-motor and supplementary motor areas, the somatosensory cortex and the posterior parietal cortex, to form the CST which is the major motor output pathway. Importantly, all of these areas reside within the middle cerebral artery territory and are frequently injured in an arterial perinatal ischemic stroke (NAIS, APPIS) but are specifically spared in PVI.

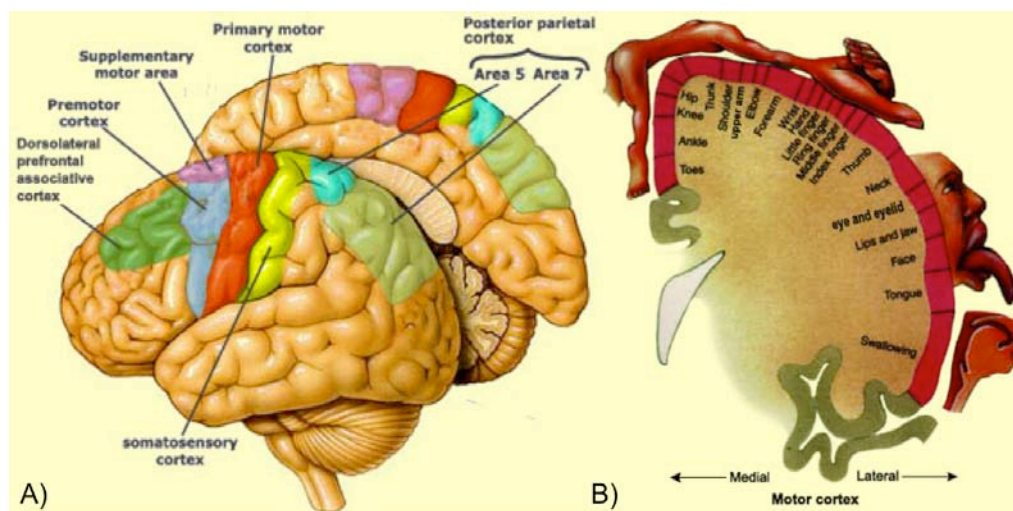


Figure 1.2. Motor cortex and homunculus. Location of the motor cortex and associated motor areas (A) and the representative somatotopic motor map (homunculus) (B).

Reprinted with permission from www.thebrain.mcgill.ca .

1.3.2 Corticospinal Tract (CST)

The CST consists of large myelinated axons of the pyramidal cells from layer 5 of the primary motor cortex that converge with fibers of the cortical areas defined above. The CST runs from

the motor cortex through to the spinal cord where it innervates specific target muscles and is responsible for conducting movement impulses from the brain to the spinal cord (Figure 1.3).

Axons of the upper motor neurons (pyramid cells) begin their descent to the spinal cord from the motor cortex by passing through the corona radiata (periventricular) and internal capsule. In the brainstem, the fibers stay ventral as they occupy the middle portion of the cerebral peduncles. The CST continues to descend along the anterior brainstem to reach the basis pontis. At this level, the fibers are more diffusely distributed and come in contact with many crossing fibers that traverse the pons. At the most caudal portion of the medulla most fibers course dorsally and cross the midline: this is known as the motor decussation. Fibers that cross over enter the lateral portion of spinal cord and are referred to as the lateral CST. The lateral CST at the upper cervical level influence lower motor neurons that innervate the neck and shoulder muscles, while the medial fibers of the lateral CST at the cervical levels influence lower motor neurons that innervate upper extremity muscles. The fibers that did not cross the midline in the medulla are called the ventral CST and usually cross over as they reach their target, influencing lower motor neurons that innervate the trunk musculature (Figure 1.3). As the fibers descend further down the spinal cord, the tract becomes considerably smaller. Lower motor neurons at the lumbosacral level of the spinal cord innervate the musculature of the leg and foot. The synaptic connections between the upper motor and lower motor neurons represent the final central output of the motor system being converted into activation of the peripheral nervous system components and resulting movement.

The CST is affected in all above mentioned stroke syndromes, resulting in a contralateral motor deficit (hemiplegic cerebral palsy). Current literature suggests these motor deficits are very prominent in perinatal stroke including 30-60% in arterial ischemic stroke,^{38,39} and 80% in

PPIS and PVI where retrospective diagnosis confers a selection bias^{6,9,10,38}. Such adverse motor outcomes are the greatest single factor impairing function and quality of life in these children. These deficits last for decades and often have limited available treatment options.

Due to the timing and quite focal nature of the injury in an otherwise healthy brain, perinatal stroke represents an ideal human model to study developmental plasticity. In turn, NAIS/APPIS and PVI provide a pairing of diseases to understand these processes, both for what they have in common (injury to the CST and motor deficits) and where they differ (location and timing of injury). New models of neuroplasticity after perinatal stroke suggest relative CST integrity is a key determinant of disability and the potential for rehabilitation. Although there is no cure for perinatal stroke, intensive and patient-specific treatment paradigms can improve day-to-day life activities⁸.

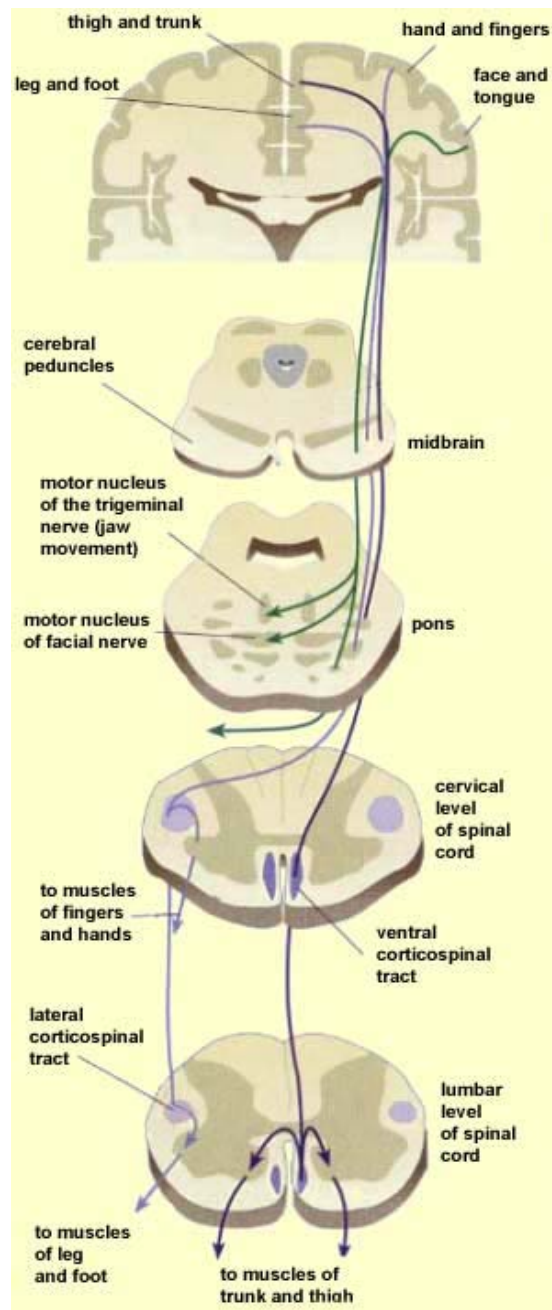


Figure 1.3. The corticospinal tract trajectory. Starting in the motor cortex, pyramidal cells converge with fibers from the associated areas and travel ventrally down through the cerebral peduncles in the midbrain through the pons. The lateral CST fibers cross at the level of the decussation of the superior cerebellar peduncle, while the ventral CST remains ipsilateral until further down the spinal cord. Reprinted with permission from www.thebrain.mcgill.ca .

1.4 Tools for Measuring Motor Outcome

There have been many advances in how motor function is assessed in children. New measures are becoming increasingly child and family friendly allowing for more specific assessment of motor function for treatment and therapy planning. Historically, many CP outcome measures focused on lower extremity function, due in part to a predominance of lower extremity involvement in other forms of CP (e.g., diplegic and quadriplegic). There are now improved and validated measures established for upper extremity function. Further, they are sensitive to the time, attentional, and behavioural focus of the children being tested. These modern outcome measures also better conform to the principles of the WHO International *Classification of Functioning, Disability, and Health* (ICF).

While these modern approaches to measuring motor dysfunction in children are applicable for studying perinatal stroke outcomes, assessments specific to perinatal stroke are lacking and therefore must be extrapolated from closely related or overlapping populations. For example, the pediatric stroke outcome measure (PSOM)⁴⁰, was designed to quantify diverse neurological outcomes across both perinatal and childhood stroke populations. Hemiparetic CP specific upper extremity measures such as the Assisting Hand Assessment (AHA)^{41,42} and Melbourne Assessment of Unilateral Upper Extremity Function (MA)⁴³ offer more functional and specific measures of fine motor abilities both bilaterally and unilaterally but have not been studied in perinatal stroke specifically. Due to the reliance on self-reporting and independent living, adult stroke outcome measures and scales are not appropriate for children. Therefore, it is a combination of these measures that currently represents the best means to quantify motor function in children with perinatal stroke.

1.4.1 Pediatric Stroke Outcome Measure (PSOM)

The PSOM is the only validated pediatric stroke outcome measure⁴⁰. It was developed at the Sick Kids Stroke Program in Toronto, Canada⁴⁰. It has been demonstrated as reliable, capable of conferring objective, disease specific, measures of neurological recovery following childhood stroke. It is not specific to motor outcome but measures neurological impairment across a multitude of areas. It is comprised of 115 test items spanning cognition, language, and cranial nerve, motor, sensory, cerebellar, and gait functions. It is useful from early infancy to late teenage years with an included option of “not age-appropriate” for each item⁴⁰. The motor function sections of the PSOM catalogue many different examination findings and summarize them in a “summary of impression” Likert scaled score as follows: 0 (normal), 0.5 (mild weakness with no functional impairment), 1 (moderate impairment), and 2 (severe impairment). For the purposes of statistical analysis, PSOM scores are often dichotomized into good and poor outcomes.

1.4.2 Assisting Hand Assessment (AHA)

The AHA is a sensitive, evidence based, reliable and valid assessment that provides objective quantification of bilateral hand function in children with hemiparesis^{41,42,44}. According to a recent systematic review⁴⁴, the AHA was the only assessment with evidence to suggest validity and reliability for assessing bimanual tasks in children less than 3 years of age. It shows the strongest evidence for inter-rater and intrarater validity, test validity, and test-retest reliability, as well as responsiveness to change, for bimanual tasks in children with hemiparesis. The AHA is administered by trained, certified occupational therapists. Tasks performed are videotaped and designed to reflect many upper extremity tasks relevant to everyday functioning. Tasks are

objectively scored and quantified into total gross (out of 88) and percentage scores. For these reasons, the AHA has emerged as the leading primary outcome measure used for clinical trials of children with hemiparesis.

1.4.3 Melbourne Assessment of Unilateral Upper Limb Function (MA)

The MA assesses the quality of upper limb function unilaterally in children. In contrast to the AHA, the MA is solely unilateral. It examines multiple items involving reach, grasp, release, and manipulation involving the affected limb. All sessions are videotaped and scoring is completed by trained occupational therapists based on criteria including range of motion, accuracy, fluency, and quality of movement⁴³. The MA is a validated and reliable measure that is able to detect therapeutic changes in hemiplegic CP⁴³.

Therefore, the combination of these three motor measures provides a robust panel of assessments of upper extremity motor function. There are other available motor function measures and are reviewed elsewhere^{44,45}. However, none are better validated and/or specific to perinatal stroke.

1.5 Magnetic Resonance Imaging (MRI)

MRI is an imaging tool primarily used in medicine that allows for detailed visualization of internal body structures. It is based on the safe interaction of radio frequency radiation and the magnetic properties of atomic nuclei in the presence of a magnetic field. Because the vast majority of MRI involves the hydrogen nucleus of a water molecule, we will restrict our MRI description to hydrogen nuclei. However, the concepts described here extend to other MR-sensitive nuclei as well.

The hydrogen nucleus contains a single proton that possesses a partial positive charge and a resulting spin (much like the Earth spins). This spin generates a small magnetic field, referred to as a “magnetic moment” that points along the axis of spin (Figure 1.4A). In our bodies, these magnetic moments are randomly oriented, such that there are zero magnetic fields associated with these nuclei. When the body is exposed to a large magnetic field (like an MR scanner) these magnetic moments tend to align either parallel or anti-parallel to the field, such that the result is a net magnetization in the direction of the large field (as an aside, to appreciate the magnitude of the magnetic field of an MR scanner, consider that the Earth’s magnetic field is approximately 0.5×10^{-5} Tesla (T). Therefore, a 1.5 T magnet is approximately 30,000 times greater than that of the Earth’s magnetic field.) Unlike a compass needle, however, the alignment is not complete, but is off-axis. As a result, there is a force (torque) on each magnetic moment causing them to rotate, or precess, about the main magnetic field at a nucleus-specific frequency in the radio frequency range, called the Larmor frequency (ω) (Figure 1.4B).

For the purposes of imaging, the net magnetization is purposefully tipped away from the direction of the scanner’s magnetic field using an additional perpendicularly oriented short-duration magnetic field tuned at the Larmor frequency (typically called a radio frequency (RF) pulse, or B1 field). This is the resonance condition. After the pulse is extinguished, a signal is recorded as the net magnetization returns to equilibrium, which occurs via two main mechanisms described in the next section.

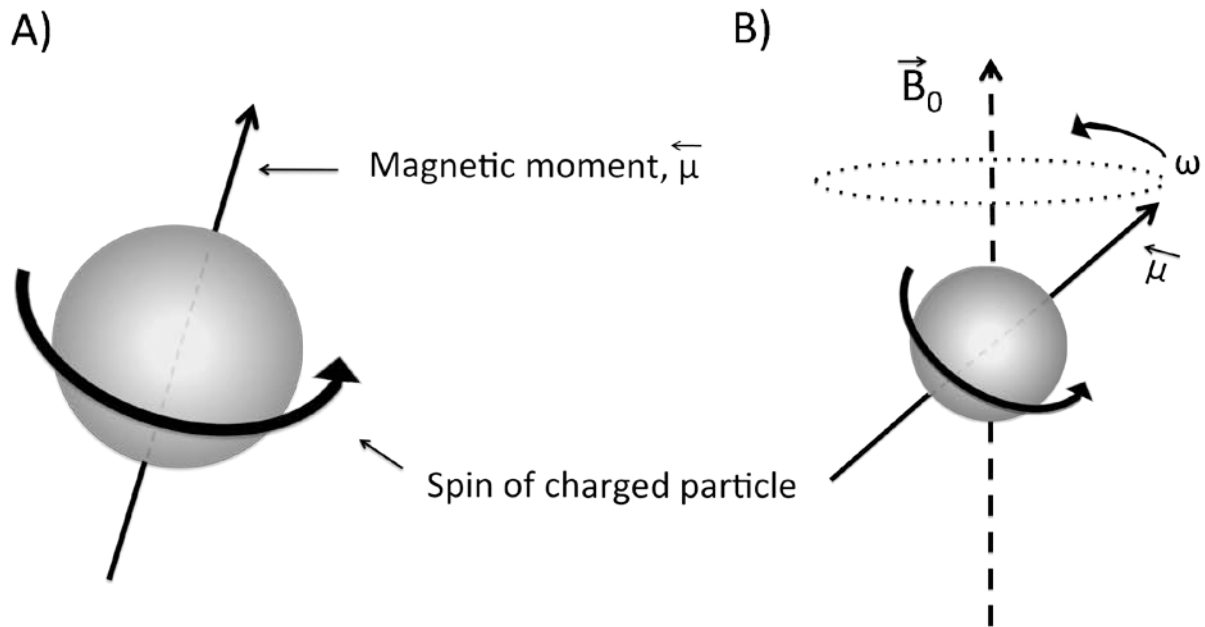


Figure 1.4. (A) The spin of the hydrogen proton generates a small magnetic moment; μ . (B) Magnetic moments precess about the main magnetic field (B_0) at a nucleus specific frequency, ω , called the Larmor frequency (B).

1.5.1 T1 Weighted and T2 Weighted MRI

T1 relaxation is also known as spin-lattice relaxation. The net magnetization returns to equilibrium by releasing energy (heat) to the surrounding environment (lattice). The return to equilibrium is exponential in nature, and the time constant that characterizes it is called T1. Hence, it is typically referred to as T1 relaxation. T1 relaxation occurs at different rates for hydrogen nuclei in different environments, for example, different tissues or chemical environments. Thus, through careful timing of an MR imaging sequence, these differences can be exploited to generate an image with contrast weighted by the T1 of the tissues of interest, i.e., a T1-weighted image.

T2 relaxation, on the other hand, is not an energy transfer, but is rather the decay in MR signal due to the differing magnetic field environments of each spin. That is, because each spin is itself a magnetic field, the net field experienced by spins within different environments will vary, thus altering their precessional frequencies, which is proportional to magnetic field. As a result, the MR signal becomes incoherent over time as the signals from each spin become more out of phase with each other. This is why T2 relaxation is sometimes referred to as spin-spin relaxation. This signal decay is also exponential in nature, and the time constant that characterizes it is called T2. As for T1, T2 is different for different tissue types, and through careful timing of an MR imaging sequence, we can exploit these differences to generate an image with contrast weighted by the T2 of the tissues of interest, i.e., a T2-weighted image.

1.6 MRI and Stroke

With recent advances in neuroimaging, recognition and the systematic study of perinatal stroke have greatly improved⁷. MRI has had widespread clinical use and is the modality of choice in the diagnosis and management of both acute and chronic ischemic perinatal stroke^{7,46}. During acute stroke there is a profound restriction of water within the affected tissues that is thought to be caused predominantly by cytotoxic edema. Additional factors that may contribute to restricted diffusion include cellular swelling and a decrease in the diffusion of low-molecular weight molecules⁴⁷. Diffusion weighted imaging (DWI) allows for the visualization of restricted diffusion (i.e., restricted random movement of water) within the brain during acute stroke. Diffusion weighted images are highly sensitive, specific, and non-invasive making them an optimal choice for acute stroke diagnosis. Therefore, the most common type of magnetic resonance imaging used to diagnose acute stroke is DWI. For the neonatal brain, DWI is the best

for detecting early ischemia and is considered the gold standard for acute, focal infarction⁷.

Within 10-14 days following tissue death a fluid-filled space remains that is visible on both T1 and T2 scans, where the tissue has died (Figure 1.5).

Furthermore, MRI has been instrumental in the diagnosis and classification of the chronic stroke (PPIS) often observed in the perinatal population^{6,10}. The availability of MRI for diagnosis of stroke has drastically improved the current understanding of the evolution of stroke. It also plays an important role in the prediction of outcome. Understanding long term effects and outcomes can help with expectations of recovery for patients and their families, and is important for planning treatment and therapy. Current literature demonstrates that conventional MRI has the ability to assess the amount of motor impairment related to lesion size and site⁴⁸⁻⁵⁰. Specifically, the integrity of the CST (measured by lesion volume) correlates significantly with the degree of motor impairment following chronic stroke in adults⁵⁰. Further, conventional imaging has been instrumental in the assessment of Wallerian degeneration within distal areas not directly connected to the lesion site, particularly the CST; this has been shown to be a significant predictor of motor outcome⁵. Others have used conventional MRI to investigate the relationship between grey matter and motor outcomes. In one study⁵¹, total grey matter volume in the brain was significantly decreased following PVI. Further, reduced grey matter density in non-infarcted motor areas is predictive of poorer motor outcome⁵².

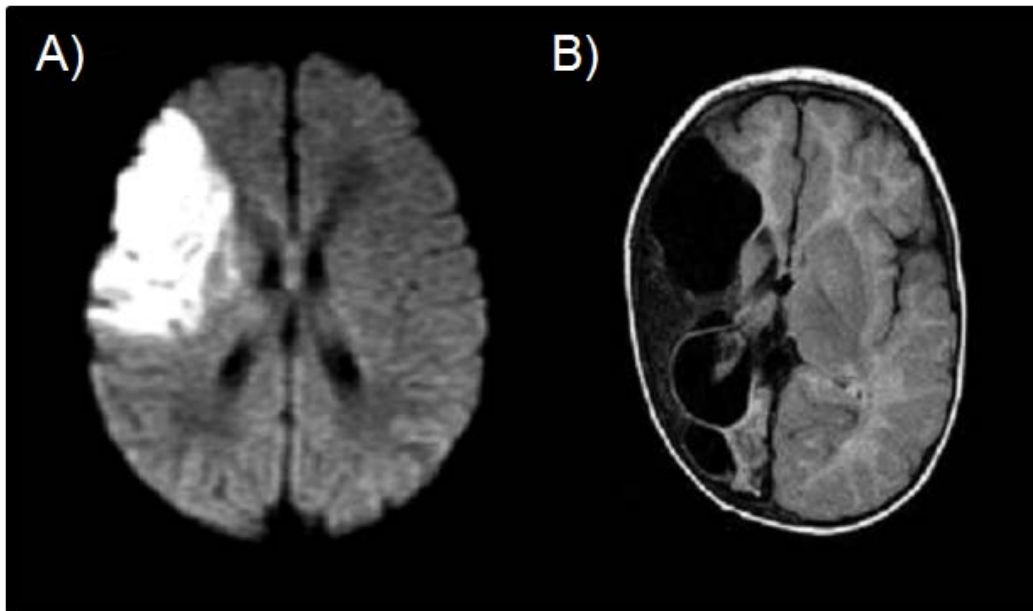


Figure 1.5. (A) Example of a DWI showing restricted diffusion due to acute right MCA arterial stroke. (B) T1 MRI showing chronic perinatal stroke in the same arterial territory.

1.7 Diffusion Weighted Imaging (DWI) and Diffusion Tensor Imaging (DTI)

Diffusion imaging relies on the random motion (micro-movements) of water molecules within tissue (diffusion), specifically within the voxels (i.e., three dimensional pixels) of the image⁵³.

The diffusion of water within tissue differs based on its environment in a measurable fashion.

Diffusion of water that occurs freely in all directions is said to be isotropic (i.e., as in cerebrospinal fluid). However, in brain tissue, the diffusion of water molecules is often highly restricted and influenced by a variety of factors such as biological barriers including cell membranes, cytoskeleton, macromolecules, and myelin. Diffusion that is restricted along certain directions in this fashion is thus referred to as anisotropic (Figure 1.6).

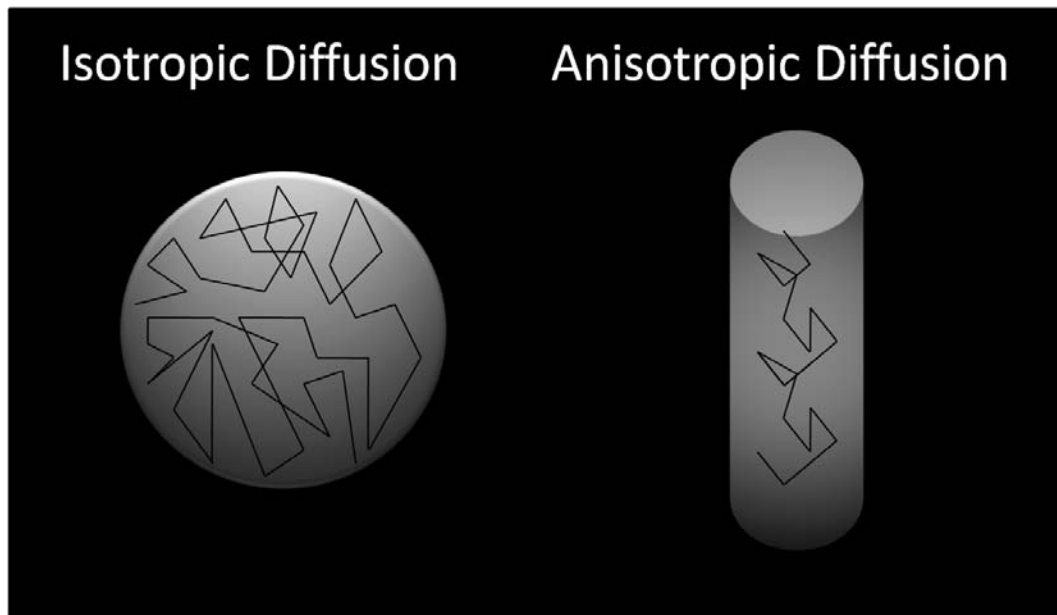


Figure 1.6. Illustration depicting diffusion within two different types of samples, one of which has similar molecular displacements in all directions (isotropic diffusion) the other having greater diffusion along one direction over another (anisotropic diffusion).

DWI is essentially a T2 sequence that is sensitized to diffusion through the application of additional gradients in specific directions (i.e., linear increases in magnetic field strength). In a typical T2 imaging sequence, signal dephasing that occurs following the excitement of the nuclei by the RF pulse (as described above) can be reversed with the subsequent application of a 180-degree RF pulse, producing another signal. Known as a spin-echo experiment, this procedure is sensitive to molecular diffusion. Because precessional frequency is determined by the local magnetic field, when a gradient field is applied, spins at different locations will precess at different frequencies (Figure 1.7B). When the gradient field is reversed some time later, the spins that remained stationary (i.e., did not diffuse) would experience no net phase change regardless of their position in the gradient (Figure 1.7D). However, non-stationary spins would experience a

net phase change directly proportional to their net displacements in the direction of the gradient during the time between the gradient and its reversal (Figure 1.7D). The result is a distribution of phases leading to a loss of signal coherence and a reduction in the signal amplitude. That is, more diffusion within a voxel leads to more dephasing, and thus a weaker signal (Figure 1.7).

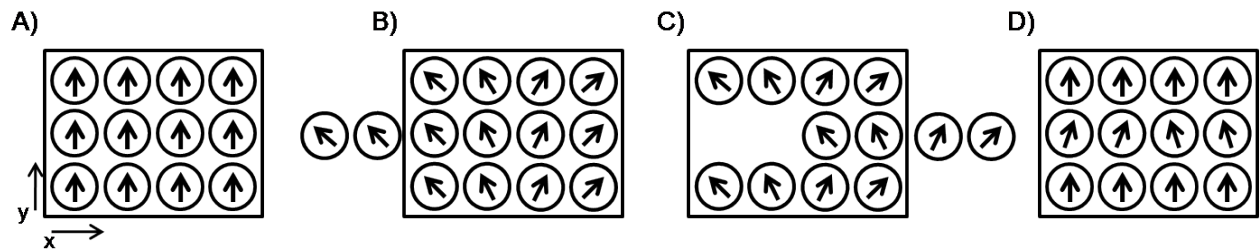


Figure 1.7. Schematic of how diffusion leads to reduced MR signal within an image voxel (represented as a square). (A) After an RF pulse is applied, all spins are in phase. (B) After application of a linear gradient in the x-direction, phase is altered as a function of x, due to the linear change in spin precessional frequency. (C) Over time, some spins diffuse (middle row) within, out of, or into the voxel. (D) After gradient reversal, spins along the middle row are not completely re-phased, due to their new x positions, leading to a reduced total voxel signal.

The amount of diffusion weighting in the resulting image depends on the characteristics of the diffusion gradients: gradient amplitude and direction, application time, and the time between the gradient and its reversal, and is expressed as the b-factor (s/mm^2). Because sensitivity is limited only to diffusion in the direction of the gradient, gradients must be applied in at least 3 orthogonal directions. With these three diffusion images the diffusion magnitude can be calculated, representing the trace image. It is necessary to have 2 diffusion sequences with different b-factors to quantify the degree of diffusion represented by the apparent diffusion

coefficient (ADC). ADC is a measure of the average diffusion of water molecules with each voxel. With values no longer dependent on T2, ADC (mm²s⁻¹) is represented as a map. A b-factor of 0 s/mm² (T2-weighted) and imaging with a b-factor of 1000 s/mm² (diffusion weighted) is typical in current practice. This application of gradients introduces a contrast mechanism that is different from the relaxation weighted MR. The resulting maps of the signal intensity are diffusion weighted images.

DTI, on the other hand, was developed to incorporate directionality into a diffusion weighted image⁵⁴. It is a relatively new neuroimaging modality that offers the unique ability to acquire microscopic information about structural connections within the brain. Specifically, DTI maps the anisotropy (described above) of water diffusion within tissues, providing a powerful tool to visualize the white matter tracts within the brain.

To determine the degree of anisotropy within neural tissue, the required minimum number of gradient directions is 6 (to cover 3D space) to create the diffusion tensor. The tensor model was developed to access the diffusion properties in anisotropic voxels where a single value is not possible due to the dependence on direction⁵⁴. The tensor is a 3 x 3 matrix of numbers characterizing water displacements in 3D:

$$D = \begin{bmatrix} D_{xx} & D_{xy} & D_{xz} \\ D_{xy} & D_{yy} & D_{yz} \\ D_{xz} & D_{yz} & D_{zz} \end{bmatrix}$$

The diagonal elements represent the diffusivity along the 3 orthogonal axes. The diffusion tensor is what synthesizes all of the data; the anisotropic coefficient and the preferred direction of diffusion. An easier way to think about the tensor is in terms of an ellipsoid (Figure 1.8).

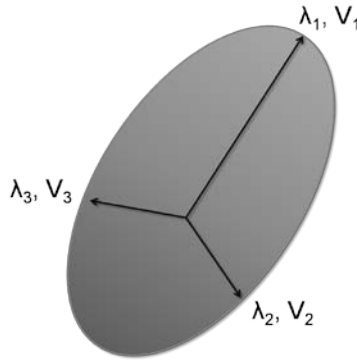


Figure 1.8. Diffusion Tensor Ellipsoid. The major eigenvalue, λ_1 , represents the direction with the greatest diffusion. λ_2 and λ_3 represent the minor eigenvalues and together they represent the water diffusion perpendicular to the major eigenvalue.

Diagonalization of the diffusion tensor is performed to calculate the eigenvalues that reflect the diffusion parallel and perpendicular within a voxel. Knowing these eigenvalues allows for water diffusion to be quantified along three directions. The largest eigenvalue (λ_1) is called the major eigenvalue, and is associated with the direction along which diffusion is the greatest (the long axis of the ellipsoid, for example along a white matter fiber tract). The two remaining and smaller eigenvalues, often referred to as the minor eigenvalues (λ_2 λ_3), represent the direction of the water diffusion orthogonal to the major eigenvalue⁵⁴⁻⁵⁶. λ_1 also represents the parallel diffusivity, also known as axial diffusivity (AD), and for our application tells us about the diffusion along the tract or axon:

$$\lambda_{\parallel} = \lambda_1$$

In contrast, the average of λ_2 and λ_3 represents the perpendicular diffusivity (λ_{\perp}), or radial

diffusivity (RD), and tells us about the diffusion across the tract:

$$\lambda_{\perp} = \frac{\lambda_2 + \lambda_3}{2}$$

The mean of all the three eigenvalues represents the mean diffusivity (MD)^{57,58}, which provides information about the average rate of diffusion within the voxel regardless of direction:

$$MD = \frac{\lambda_1 + \lambda_2 + \lambda_3}{3}$$

The parallel and perpendicular diffusivities, along with the mean diffusivity allow for fractional anisotropy (FA) to be calculated, which is a measure of the degree of which water diffusion is directional. Zero indicates completely isotropic and one (1) indicates completely anisotropic diffusion⁵⁹.

$$FA = \frac{\sqrt{3} \sqrt{(\lambda_1 - \lambda)^2 + (\lambda_2 - \lambda)^2 + (\lambda_3 - \lambda)^2}}{\sqrt{\lambda_1^2 + \lambda_2^2 + \lambda_3^2}}$$

An example of an FA image is shown in Figure 1.9A. White matter tracts in the brain are highly directional and appear hyperintense on FA maps, while less directional grey matter will appear relatively black. Further, in areas where the apparent diffusion is high, the subsequent FA values will be low (approach 0). While the FA map provides information about the magnitude of the anisotropy, it does not specifically indicate the direction of the diffusion. Thus, typically coded images are also generated (orientation based color coding). Figure 1.9B shows how the color FA maps utilize a red-blue-green color scheme, to describe the predominant diffusion direction. Moreover, the color map also helps to visualize diffusion anisotropy (image brightness)⁶⁰. Tractography and ROI analysis can then be performed using the different anisotropy maps.

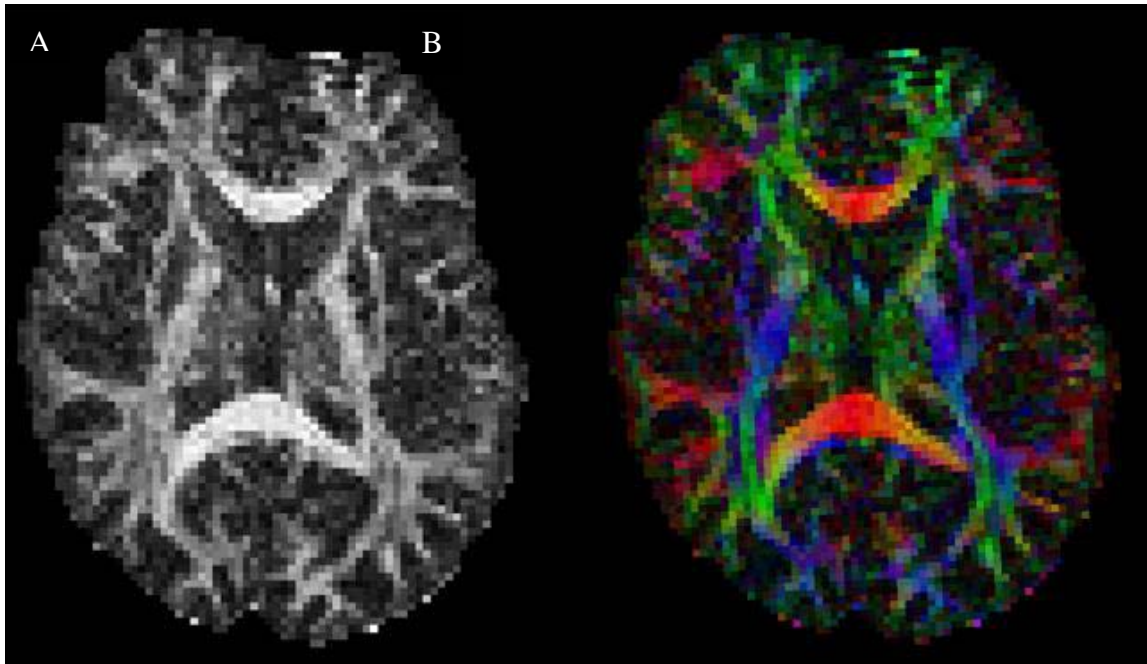


Figure 1.9. Illustration showing two types of FA images, greyscale (A) and color (B).Anterior-posterior is labelled green, the medial-lateral direction is red, and the superior-inferior direction is labelled blue.

Because DTI is able to provide unique structural and physiological information, it has been used to study both the developing and mature brain and in many diseases states⁵³. Specifically, DTI provides a non-invasive way to look at neural fiber composition, integrity, and orientation within the brain that is not possible with other imaging methods⁵⁹. To date, DTI tractography has been successfully used to study large white matter tracts including the CST, the limbic arches, corpus callosum, inferior fronto-occipital fasciculus, inferior longitudinal fasciculus, and superior longitudinal fasciculus⁶¹. In children, DTI has been shown to be effective in the study of white matter diseases such as trauma, brain tumor, demyelinating disorders, and congenital brain malformations such as callosal agenesis⁶¹. Multiple approaches to utilizing DTI have been developed.

1.7.1 Cross-sectional Analysis (Region of Interest)

The cross-sectional analysis, or region of interest (ROI), method is simple and easy to perform. In this method, a two- or three-dimensional region is manually drawn around the area of interest. Alternatively, a fixed sized shape (often a circle or square) can be placed in the area of interest. All of the voxels within the region are then averaged to provide a single measurement. A disadvantage of this method is that each ROI needs to be placed manually for each patient, making this a time consuming and user-dependent process. It also lacks the functional specificity of defined brain tracts.

1.7.2 Track- based Analysis (Tractography)

Axons within the brain that share similar destinations bundle together forming larger white matter tracts. DTI tractography is a procedure used to non-invasively visualize two- or three-dimensional reconstructions of white matter tracts/fibers within the brain by quantifying diffusion properties^{60,62}. Tractography and fiber tracking algorithms operate based on voxel-wise information provided by DTI to infer connections between adjacent voxels presumably belonging to the same tract. Unique to DTI, visualization of connectivity between structures within the brain is possible using tractography. While potentially very valuable, it is also important to understand the limitations of tractography and its properties.

Using the tensor model there are two types of fiber tracking approaches possible: deterministic streamline and probabilistic. Both methods are made possible by taking advantage of mathematical algorithms that rely on the availability of estimates of the orientation of white matter fibers. The principle diffusion direction (major eigenvalue) within each diffusion voxel is assumed to provide a suitable orientation estimate. FACT (fiber assignment by continuous

tracking) was one of the first deterministic algorithms developed^{60,63}. FACT uses a “nearest-neighbour” interpolation where the desired white matter orientation is approximated as that of the nearest voxel. Tracking is then propagated in a step-wise fashion along the orientation estimated at that point (Figure 1.10). Other interpolation methods and propagation algorithms of deterministic tractography are reviewed elsewhere⁶³.

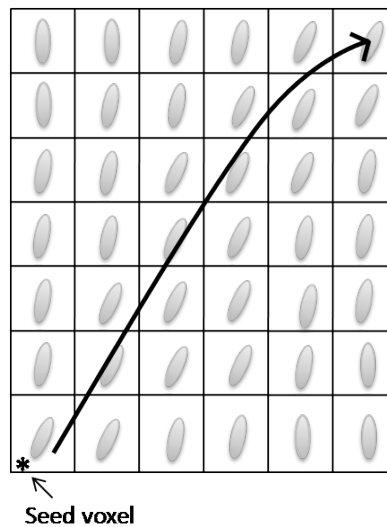


Figure 1.10. Fiber assignment by continuous tracking (FACT) method. Fiber tracking initiates within a ROI or seed voxel. Tract propagation follows the vector alignment of the ellipsoids.

Designating a minimum of two regions of interest generates tracts. Tracking is terminated when stop criteria are reached, typically based on a diffusion measure like FA. When the anisotropy within a pixel falls below a predetermined value (e.g., $FA < 0.2$), tract propagation ends. FA is often used as a criterion for several reasons. In regions of low anisotropy, the major eigenvector of the diffusion tensor will be poorly estimated due to noise and as anisotropy tends to be high in white matter and low in grey matter, a sudden decrease in the diffusion anisotropy is suggestive of a boundary between white and grey matter. An additional termination criterion is

to set a threshold angle between two continuous vectors. If the angle between two voxels exceeds the threshold, tract propagation ends. The deterministic method produces one reconstructed tract per seed point and cannot depict branching fibers, a major disadvantage for deterministic approaches⁶⁴. For example, the CST at the level of the centrum semiovale should produce a fan-shaped configuration, which is often not reproduced with this method due to multiple crossing fibers. Possible reasons for this are that when one corrupt orientation estimate is encountered there is the potential of the tracking algorithm to venture off course into an adjacent white matter structure, resulting in false-positive and false negative connections⁶³, and that white matter tracts traverse large numbers of voxels making them more vulnerable to cross paths with other white matter tracts (crossing fibers). One advantage of this method is that it uses a semi-automated approach, where the tract-selection regions can be loosely defined, meaning that the user does not need to outline the structure of interest precisely but rather provide one (or more) areas through which the tract of interest must pass, thereby, minimizing user dependence.

A drawback of deterministic algorithms is that they only provide one estimate of the path of the white matter tract without taking into consideration the confidence interval around this estimate. In contrast, probabilistic approaches aim to mediate these problems by considering multiple pathways stemming from one seed point, a probability distribution, and from each point along the trajectory. This ultimately accounts for the uncertainty in the estimation of fiber direction seen in the deterministic approach. In addition, the probabilistic approach is also resistant to noise, a benefit for images that have a limited signal to noise ratio. However, there are drawbacks associated with the probabilistic methods; it is slower and not as interactive for the user, and the results are harder to interpret visually as it generates a three dimensional

volume of potential connectivity's as opposed to discrete geometric pathways requiring greater anatomical knowledge on the part of the user.

The streamline deterministic approach was used for fiber tracking in this study. Fortunately, the disadvantages mentioned above are not as severe in dominant tracts like the CST because the orientation produced by the diffusion tensor model is fairly close to the largest contributing fiber direction. Therefore, tensor based tractography algorithms, like FACT, are able to follow the CST through known areas of crossing fibers (pons and centrum semiovale)⁶⁵.

1.8 DTI and Stroke

Over the last decade there has been a significant increase in the number of studies using DTI to investigate neurological disease. Studies have investigated specific diffusion variables within a lesion compared to healthy brain, in order to determine correlations with outcomes^{50,66-68}.

Within the adult stroke population, it is known that decreased FA values and increased directional diffusivities are present in the lesioned CST of chronic stroke patients compared to controls⁶⁷. Investigations of CST integrity with DTI and motor outcome in the adult stroke population suggest that relative CST integrity is directly correlated with motor outcome, and that diffusion measures provide valid structural markers of this integrity⁶⁹⁻⁷¹.

Further, it has been suggested that CST integrity in acute imaging may also be predictive of long term outcomes^{69,70,72}. Interestingly, these findings seem to be consistent using either tractography based methods or ROI methods. Tractography⁶⁷ and ROI^{66,72} based studies assessing the CST following stroke both hold promise for prediction of outcome. Although comparative studies of the two methodologies are lacking, some research suggest that the full tract analysis of FA may prove a more valuable tool than the well described ROI analysis⁶⁷ while

others suggest that both methods are reliable and provide complimentary rather than redundant information⁶⁸.

Recently, DTI has been used to investigate how the diffusion variables change across the lifespan in healthy populations^{73,74}. Generally, FA increases within most white matter tracts during childhood and adolescence, reaching a peak sometime during the mid-twenties to forties and then decreases while MD shows the opposite trend, decreasing from childhood to late adolescence reaching a low between 20-40 years and then steadily increasing through later adulthood. Changes in the perpendicular diffusivity drives the changes in FA, suggesting a change in myelin or axonal density⁷³. Another study⁷⁴ found age related decreases in the parallel, perpendicular and mean diffusivities in major white matter pathways in healthy subjects.

Within the infant and child literature specifically, studies combining fMRI, DTI and transcranial magnetic stimulation (TMS) have found evidence of cortical re-organization of the sensorimotor system as well as the language system in children with periventricular lesions⁷⁵. Periventricular leukomalacia⁷⁶, CP⁷⁷ and congenital hemiparesis^{57,58,78} studies have reported DTI (FA, RD, and MD) to be a useful tool for predicting motor outcomes in children.

There have only been a few recent studies specifically looking at DTI in perinatal stroke. Most have been concerned with non-motor areas, such as the language area, which show evidence of re-organization⁷⁹. Furthermore, there is evidence from non-specific congenital hemiparesis studies in children that asymmetry of FA, MD and RD in the corticospinal tracts correlates with the severity of motor dysfunction^{57,58,78}. Unfortunately, perinatal stroke data is lacking. While perinatal stroke does possess some commonalities with adult stroke, the specific timing and the continued brain development post-stroke do not permit a direct comparison. Hence, there is a need for perinatal stroke specific studies to better our understanding of recovery

and outcome in children. A recent study that looked specifically at focal perinatal injury (AIS and hemorrhagic stroke) showed similar findings to what have been observed in adult stroke studies. Specifically, hemispheric asymmetry in diffusion parameters is significantly different from those in a healthy population of age-matched children and correlates with motor outcome (hemiplegia)⁴⁶.

To date, DTI has not been used to systematically investigate CST integrity or damage in children with motor deficits secondary to perinatal stroke. It has been suggested that following perinatal ischemic stroke there is damage to the CST descending from the lesioned hemisphere. This has been supported by investigating diffusion properties within the CST in the adult stroke population and in children with hemiparetic CP. Often it is decreases in FA and AD with increases in RD that reflect damage within white matter tissue that characteristically reflects decreased integrity^{57,64,78,80}. More research is needed in the area of perinatal stroke and CST integrity in order to validate tractography and ROI analysis methods as reliable tools for predicting motor outcome have not been established and many questions remain unanswered. Are diffusion parameters different between lesioned CST and non-lesioned CST after perinatal stroke? Can diffusion parameters within the affected CST help predict motor outcome in perinatal stroke? Is there a specific diffusion parameter, for example RD or FA that is better at predicting long-term motor outcome? Finally, is tractography more useful for investigating CST integrity than ROI analysis?

Therefore, our study is the first to our knowledge that aims to investigate specifically CST integrity and damage following perinatal ischemic stroke causing hemiparesis. Our first goal was to confirm that diffusion parameters are measurable in the CST and differ between the lesioned and non-lesioned hemispheres. Most studies investigating damage of the CST using a

variety of injury models have focused on either a single ROI analysis or a full tract. Because our population is often left with a large lesions post-stroke, or stroke has occurred in the direct path of the CST, it is not always possible reconstruct a complete CST on the lesioned side. Therefore, we developed a method to analyze multiple segments of the CST and a single ROI along the tract. Our subsequent goals were to determine if any differences between segments of the CST and their association with motor outcome.

1.9 Aims and Hypotheses

Aim 1 - Quantify and compare the diffusion parameters between the lesioned and non-lesioned CSTs in children with perinatal stroke.

Hypothesis: All diffusion parameters within the lesioned CST differ from the non-lesioned CST in children with perinatal stroke.

Aim 2 – Compare diffusion parameters within different segments of the CST.

Hypothesis: A defined subtract of the lower CST will provide the most reliable diffusion measurements.

Aim 3 – Determine the associations between CST diffusion measures and motor outcome.

Hypothesis: RD of the CST partial tract will have the strongest association with poor motor outcome.

CHAPTER 2 - METHODS

2. Patient Population

All patients were enrolled through the Alberta Perinatal Stroke Project (APSP). The APSP is a population-based registry designed to identify and enrol all children in Alberta with perinatal stroke. Based at the Alberta Children's Hospital (ACH), Calgary, Alberta, Canada, the APSP is currently establishing the largest population based perinatal stroke cohort to date. Identification of potential patients is a two-fold process including prospective ascertainment since 2007 and a retrospective enrolment (1992-2007) by a comprehensive search of the International Classification of Disease codes (ICD-9 and ICD-10) and institutional databases to identify potential perinatal stroke patients. At this time, the southern Alberta cohort includes over 150 children that have been diagnosed with APPIS (42), NAIS (55), and PVI (58).

All stroke diagnoses were confirmed by modern neuroimaging (MRI) as assessed by the principle investigator pediatric neurologist and pediatric neuroradiologist. The classification of stroke was done according to previously validated⁶ criteria. The arterial lesions (NAIS and APPIS) were sub-classified according to predefined validated criteria that include the lesioned branch of the MCA as follows:

- A. Proximal M1 (PM1): includes cortical MCA areas and complete involvement of the basal ganglia supplied by MCA (e.g., putamen, globus pallidus, and caudate body).
- B. Distal M1 (DM1): includes involvement of diffuse cortical MCA areas with complete or nearly complete sparing of basal ganglia.
- C. Anterior trunk (AT): includes spared basal ganglia and only the anterior division of the MCA cortical areas affected (e.g. front lobe).
- D. Posterior trunk (PT): includes spared basal ganglia and the posterior division of MCA cortical areas affected (e.g. parietal and posterior temporal lobes).

Confirmation of the PVI lesions by validated criteria included an isolated infarction of the periventricular white matter with sparing of the basal ganglia, cortex, and immediate subcortical white matter, and evidence of remote hemorrhage (e.g., blood product) within the involuted germinal matrix visible on gradient echo or susceptibility-weighted images.

Patients for the current study were recruited during visits to the ACH Pediatric Stroke clinic by a trained research assistant or team investigator. This study was approved by the Conjoint Health Research Ethics Board of the University of Calgary. All children provided parental written informed consent. To be included in the present study, patients had to have an MRI –confirmed diagnosis of perinatal stroke (NAIS, APPIS, or PVI) in an area expected to affect motor function (e.g., arterial ischemic stroke in MCA territory) or a motor deficit (PSOM motor score >0), born at term (>36 weeks gestation), age at imaging 12 months to 18 years. Patients with bilateral or multifocal stroke or any additional neurological disorders were excluded.

2.1.1. Motor Outcomes

The PSOM data used for this study were collected by a pediatric neurologist during the patient's clinic visit. Many patients were also involved in an on-going randomized clinical trial (PLASTIC CHAMPS, <http://www.clinicaltrials.gov/ct2/show/NCT01189058>) where they received AHA and MA evaluations performed in a standardized blinded fashion by an experienced occupational therapist certified in the administration and interpretation of the tests.

2.1.2 Data Collection and Management

All data collected within the APSP (demographics, neuroimaging, neurophysiology, risk factors, and outcomes) is done according to institutional protocols and securely stored.

2.2 Image Acquisition

Images were acquired using a Siemens Avanto 1.5T MRI scanner (Siemens Medical Systems, Erlangen, Germany). Total imaging time was approximately 30 minutes. Parameters for T1 are as follows: TR = 531-580 (# of slices dependent), TE = 15, field of view 220mm², matrix of 256 x 192, and a TA of 1m30s to 3m. MP-Rage parameters were as follows: TR = 2400, TE = 4.5 TI 1000, FOV 256mm², matrix of 256 x 256, and a TA of 5m35s or 7m35s. DTI was acquired using a spin-echo, single shot echo-planar imaging sequence with the following parameters: 40-53 3mm thick slices with no inter-slice gap, TR= 5500 -7200ms, TE = 90ms, field of view 256 x 256 mm², matrix of 128x128resulting in a 2x2x3 mm³voxel size. Six non-collinear diffusion encoding directions were acquired with b = 0 and b = 1000 s/mm² according to the gradient scheme [Gx, Gy, Gz] = ([1 0 1], [-1 0 1], [0 1 1], [0 -1 1], [1 1 0], [-1 1 0]). Six averages were performed for each gradient direction and the non-diffusion weighted (b = 0 s/mm²). Total DTI acquisition time was approximately 4 minutes. These and the subsequently described DTI methods were based on an extensive review of the literature and expert consultation (Dr. Christian Beaulieu, University of Alberta, private communication).

2.3 Image Analysis

DTI analysis was in collaboration with regional and provincial DTI experts. All raw DTI images were transferred to a MacIntosh computer workstation running a parallel Windows operating

system to allow use of several different software packages. Initial analysis, tractography, and ROI analysis of the DTI images (described below) were completed with *DTIStudio* software (available at <http://cmrm.med.jhmi.edu>). Tract segmentation was completed using an in house program (Quantract)⁸¹.

2.3.1 *DTIStudio Methods*

*DTIStudio*⁵⁶ utilizes three main ROI-based boolean operations for flexible and versatile fiber selections. The “OR” operation or the union function is used for the placement of the initial seed ROI. The second operation “AND” also known as intersection, is used to capture the tracts that run through two ROIs simultaneously and will restrict the fibers from the first ROI to only those that run through the first and second ROI’s. The “AND” operation is also used for the placement of the second ROI. Finally, the third operation, “NOT”, or the exclusion function, is used to eliminate fibers that do not show the characteristic trajectory desired (trimming)^{56,60,62}.

Prior to diagonalization of the diffusion tensor, raw images were visually inspected for apparent artifacts, and images containing artifact were removed. Diagonalization of the tensor was performed to generate the six components of the diffusion tensor (Dxx, Dyy, Dzz, Dxy, Dxz, Dyx), three eigenvalues and eigenvectors, and the anisotropy maps (greyscale and orientation color-coded fractional anisotropy). The $b = 0$, mean $b = 0$, FA, eigenvalue 1, 2, and 3 maps, radial diffusivity, and trace maps were saved.

2.3.2 *Fiber Tracking Method*

Streamline tractography of the CST was performed using the fiber assignment by continuous tracking (FACT) algorithm in *DTIStudio*. Using the FACT method, the trajectory of the fiber

tracking follows the primary eigenvector from voxel to voxel. An FA threshold of 0.2 and an angle threshold of 50° ⁶² were chosen for tract propagation. Consistent with recent studies^{60,62,77} we employed a two-ROI approach to generate the tracts. ROI placement was based on existing knowledge of anatomical track trajectories for the CST^{60,62,77}. As a preliminary step to ensure tractography could be performed in our population, fiber tracking was first attempted in the non-lesioned hemisphere. The patient was excluded if the CST could not be reliably generated on the contralesional side. All tractography was completed on the directionally color-encoded FA map one hemisphere at a time. The first ROI was placed in the cerebral peduncle at the level of the decussation of the superior cerebellar peduncle (DSCP). Consistent with published CST DTI studies, this landmark is established as the focal red signal in the midline of the midbrain tegmentum on the colour FA map (see Figure 2.1A below). A second ROI was defined in the posterior limb of the internal capsule (PLIC) (Figure 2.1). Coloured blue the PLIC is easy to detect and the ROI was traced around the entire area (see Figure 2.1C below). Any CST fiber that deviated from the known trajectory; cerebral cortex through the corona radiata and PLIC down to the brainstem was trimmed using the “NOT” function and recorded. The fibers that intersected both ROIs were saved and kept for analysis.

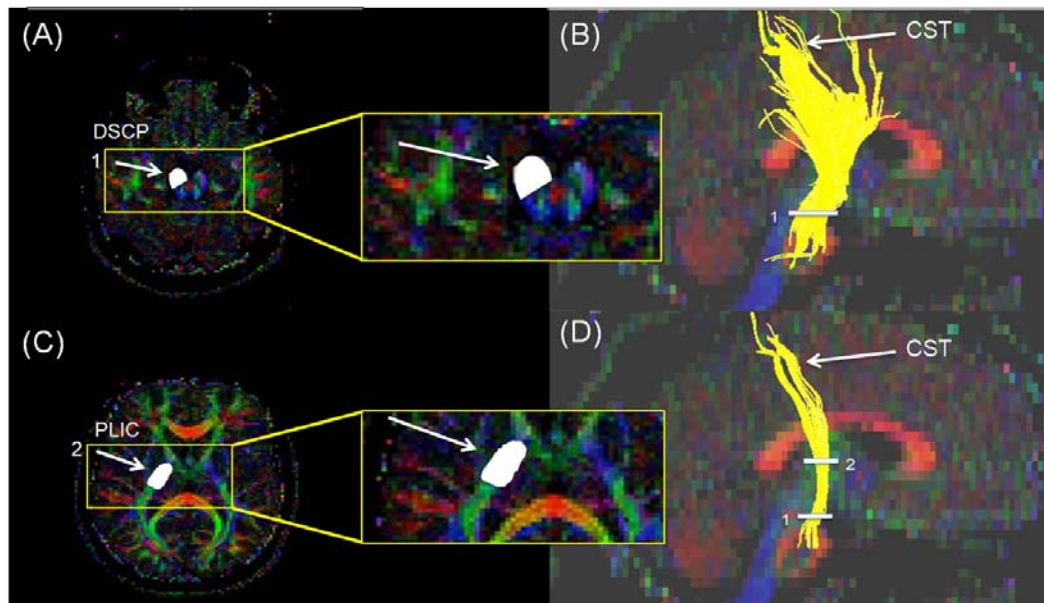


Figure 2.1. Tractography Method. Locations of the ROIs on axial slices (A and C) and the mid-sagittal slice (B and D). The first ROI is drawn on the cerebral peduncle at the level of the decussation of the superior cerebellar peduncles (DSCP). From the tracking results, the posterior limb of the internal capsule is identified. Using the axial slice, the second ROI is selected and the CST is tracked.

The saved CST tracts were loaded into Quantract⁸¹, and segmentation of the tracts into partial and mini tracts was performed. Segmentation created four tracts for the fiber tracking analysis: the full tract (FT), partial tract (PT), the upper tract (UT), and the mini tract (MT) (Figure 2.2).

- A. Full tract (FT, Figure 2.2A). All fibers that passed through and extended between the seed and the joining ROI. A version of the FT is used in most of the literature.
- B. Partial tract (PT, Figure 2.2B). The common portion of CST between the cerebral peduncle and PLIC. This avoids complications arising from cortical lesions. It is defined as the section of the CST that was between the seed (cerebral peduncle) and joining ROI (PLIC) only.

C. Upper tract (UT, Figure 2.2C). Portion of the CST above the PLIC only. It is unknown if such tracts represent “surviving” upper motor neurons above a lesion (e.g., “healthy” or uninjured CST) or not. If true, these areas would be expected to have similar DTI properties to homologous regions on the non-lesioned side.

D. Mini-tract (MT, Figure 2.2D). As some children with large lesions do not have a CST that extends completely between the two ROIs, we designed a new way to bring them into the comparison. The mini tract was limited to only the fibers that were between the seed ROI (cerebral peduncle) and one slice superior to this. This allowed us to include every participant and analyze a small portion of the CST.

FA, AD, RD, and MD were measured in each of the above tracts in each hemisphere. Each parameter was then expressed as a symmetry index (SI), defined as the ratio of the lesioned hemisphere to the non-lesioned hemisphere. For the purpose of this thesis, it was assumed that the non-lesioned hemisphere in these patients was healthy⁵⁸ (see discussion).

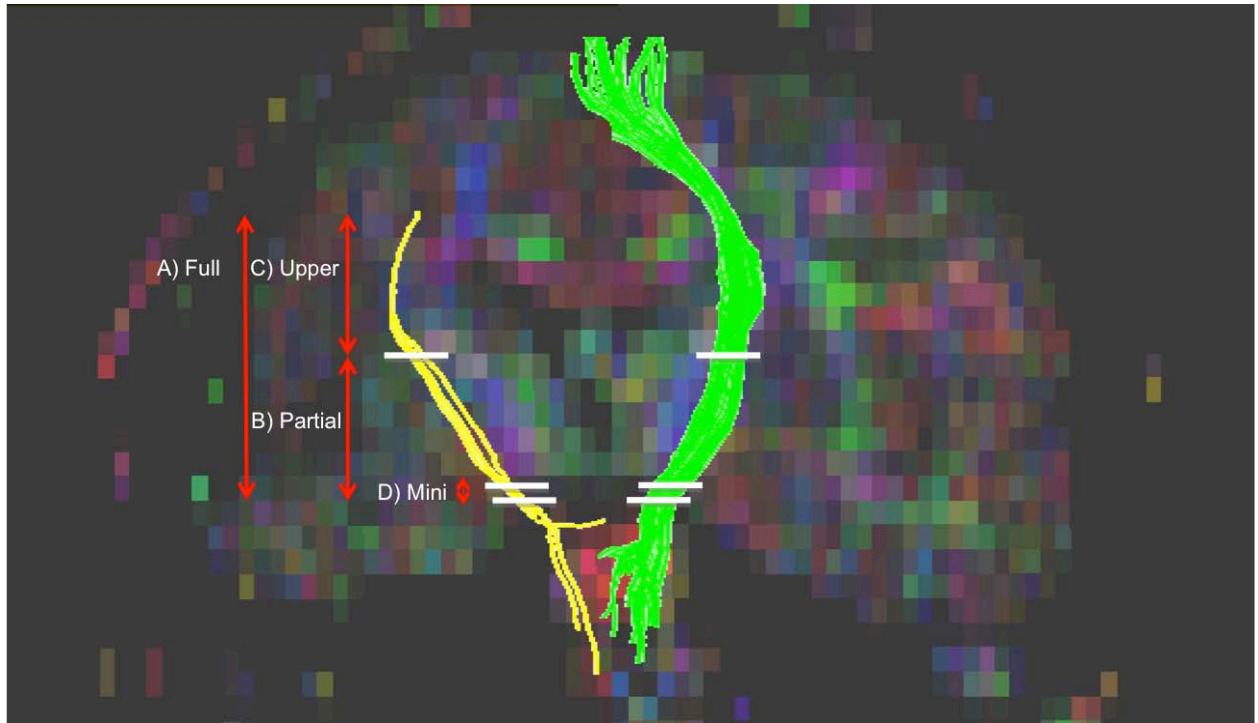


Figure 2.2. Tract segments used for analysis. An example image showing a lesioned CST full tract (yellow) and a healthy CST full tract (green). The tract segments are labelled: full (A), partial (B), upper (C), and mini (D).

2.3.3 Quantification of Diffusion Variables within the Cerebral Peduncle

A single ROI was set in each hemisphere of the midbrain CST (cerebral peduncle). The axial level chosen was based on the decussation of the superior cerebellar peduncle on the color FA map in *DTIStudio* (Figure 2.3). A circular ROI of fixed size (9mm^2) was used to limit subjectivity of the measurement and to ensure the same area was being compared in the lesioned and non-lesioned CST. We called this method “ROI measurement”. Because all of the quantitative diffusion maps are spatially aligned with *DTIStudio*, the same ROI can operate on each map simultaneously. We then used the values from the FA and eigenvalue maps to generate measurements for FA, AD, RD, and MD. SIs were calculated for each diffusion parameter.

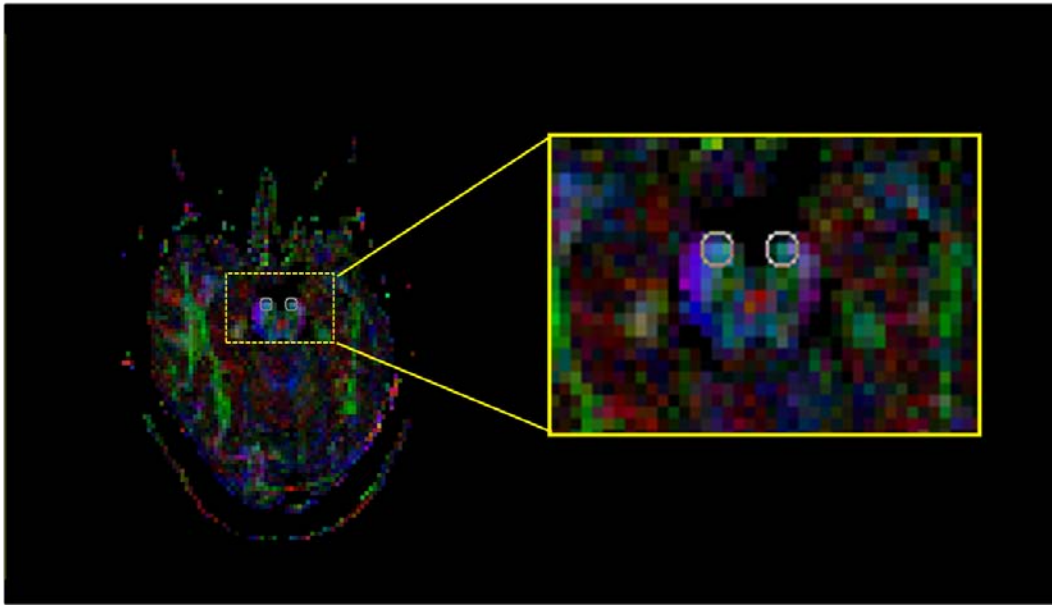


Figure 2.3. ROI Analysis. Example of where the ROI was placed for diffusion analysis. ROI was $3 \times 3 \text{ mm}^2$.

2.3.4 Quantification of the Ventral Midbrain Area at the Level of the Superior Midbrain

To confirm existing knowledge of resulting white matter damage distal to the lesion, ventral midbrain area measurements were taken for both cerebral peduncles for each patient in *Osirix* (www.osirix-viewer.com). Left and right cerebral peduncles were traced using the pencil feature separately on the uppermost axial slice in the midbrain. Axial MPAGE or other available T1-weighted images were used for this analysis. Asymmetry index was calculated as follows: lesion area/non-lesioned area (Figure 2.4).

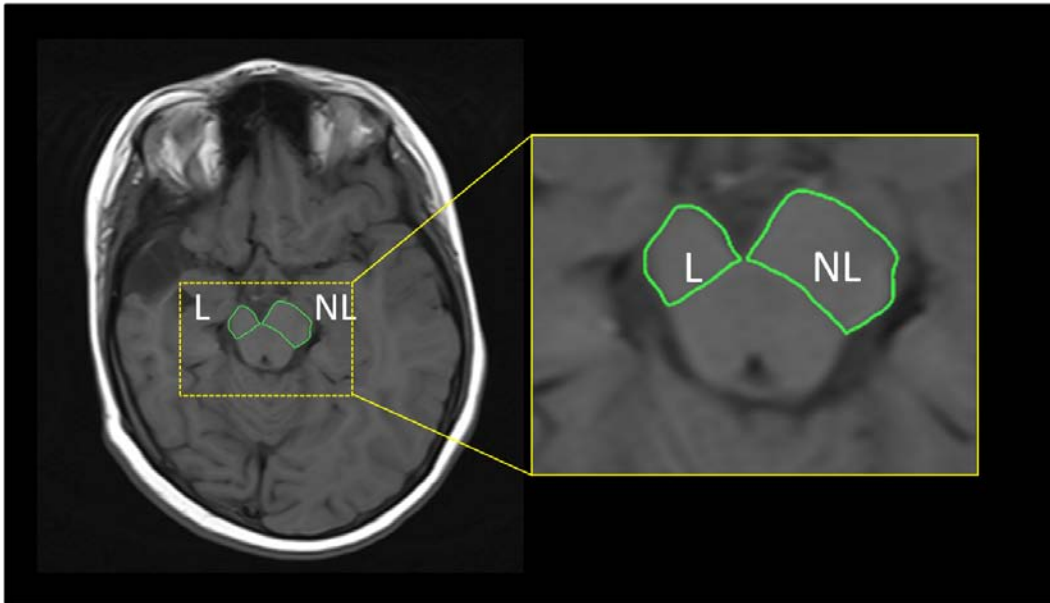


Figure 2.4. Ventral Midbrain Volume Method. The entire area of the cerebral peduncles was traced bilaterally. L represents the lesioned cerebral peduncle while NL represents the non-lesioned.

2.4 Statistical Analysis and Sample Size

2.4.1 Intra-rater Reliability

Due to the subjective nature of ROI placement and to insure reproducibility of the tractography procedure outlined above, four trials of the tractography procedure were completed for the lesioned and non-lesioned CST in 11 patients. The intraclass correlation coefficient was calculated and used to assess intra-rater repeatability.

2.4.2 Distributions and Outliers

Prior to analysis, all data were visually inspected by boxplot analysis. Outliers were identified and extreme outlier values (> 2 standard deviations (SD) from mean) were confirmed for accuracy and removed. All outliers were recorded and accounted for by dataset (see results).

Data was examined for distribution normality using the Shapiro-Wilk test. These examinations were performed across all primary data sets. If normality was violated, non-parametric versions of the above tests were also performed. These results are specifically presented at the end of the results section.

2.4.3 Primary Analysis

A paired-sample t-test was used to compare the lesioned and non-lesioned FA, AD, RD, MD, and volumes (significant with $p < 0.05$). Differences in diffusion symmetry (SI) for each variable were compared between the full, upper, partial, mini, and ROI segments of the CST using a one-way ANOVA. Prior to analysis, homogeneity of variances was assessed by the Levene's Test of Homogeneity of Variances. For ANOVAs demonstrating a significant difference between groups ($p < 0.05$), post-hoc pair-wise comparisons were then completed (Games-Howell).

2.4.4 Correlation of Diffusion Variables with Motor Outcome

Independent t-tests were used to investigate the differences in the mean symmetry of each diffusion variable between severe or non-severe motor outcome (dichotomized PSOM scores).

The independent variable was the symmetry ratio. The dependent variables were the PSOM dichotomized into severe (PSOM = 2) and non-severe (PSOM = 0 – 1.0) hemiparesis.

Spearman's Rank Order Correlation was used to investigate possible associations between diffusion variable symmetry and the AHA and MA motor outcome scores. The assumption of a monotonic relationship was visually inspected using scatterplots. This was performed across each of the defined tracts (FT, UT, PT, and MT) and the ROI analysis.

The possible effect of multiple comparisons was considered. However, with defined hypotheses made a priori, including the expected direction of effect, and the ability to compare multiple measures and tracts for consistency of effects, we determined that traditional methods (e.g. Bonferonni) were excessively conservative and not required. Statistical analysis was performed using SPSS 19.0.

2.4.5 Sample Size Calculation

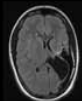
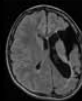

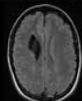


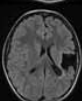
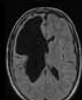
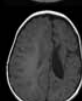
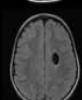

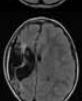

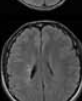
A previous case-control study of DTI in children with congenital hemiplegia⁵⁸ demonstrated an average ipsilesional decrease of approximately 35% (SD = 5) in FA values in children with poor outcome. Another DTI study in children with CP⁷⁷ found mean tract FA values of 0.5 with typical SD of 0.05. Based on these comparable studies and using a type I error of 0.05 and power of 90%, we estimated that a sample of 16 patients would be required to address our hypotheses.

CHAPTER 3 – RESULTS

3. Population

From an initial potentially eligible APSP population of 155 children, 42 children were initially identified and recruited. In 2 patients, the DTI protocol was missed, 3 patients received the incorrect DTI protocol, in 4 patients we were unable to complete the MRI, 3 patients had a diagnosis other than stroke, and 1 patient had an unexpected finding of bilateral stroke. In an additional 3 children, unanticipated technical difficulty was encountered in tracking the CST reliably in the healthy hemisphere. As results from either hemisphere could not be considered reliable in these patients, they were excluded.

The final study population is summarized in Table 1. The sample consisted of 26 children, 10 males and 16 females, with a mean age of 10.2 ± 4.2 years at imaging (range 1 – 17 years). Stroke type distribution was 14 AIS and 12 PVI. The AIS population included 2 NAIS and 12 APPIS with vascular distributions as follows: 4 PM1, 8 DM1, 1 PT, and 1 AT. All patients had PSOM scores with median age at PSOM of 10 ± 4.5 years. Distribution of motor outcomes included PSOM motor score of 0-0.5 (mild) in 4, 1.0 (moderate) in 9, and 2 (severe) in 13. Sixteen children also had AHA and MA scores with median scores of 65.5 ± 16.5 and 76 ± 18.9 respectively. All children had full, mini and ROI tract segments. Three children did not have CST in the lesioned hemisphere between the cerebral peduncle and PLIC accounting for the decreased number (23) of children with a partial tract. In 22 of the children it was possible to tract CST above the PLIC in the lesioned hemisphere resulting in the upper tract segment.

Case	Gender	Age at MR Imaging (yrs)	PSOM Motor	Stroke Type	AHA Motor	MA Motor	Image
1	Female	13	2	L. DM1 MCA	54	54	
2	Male	13	2	L. DM1 MCA	47	55	
3	Male	10	0.5	R. DM1 MCA	74	76	
4	Female	16	0.5	R. PVI	88	89	
7	Male	17	2	L. PVI	76	87	
8	Female	7	1	R. PM1 MCA	49	61	
9	Male	9	1	L. DM1 MCA	63	76	
11	Male	15	2	R. PM1 MCA	39	37	
12	Female	1	2	L. PM1 MCA	NA	NA	
13	Female	12	2	L. PVI	71	81	
14	Male	1	1	L. PVI	83	85	
17	Male	7	2	R. PM1 MCA	43	36	
18	Male	5	1	L. DM1 MCA	NA	NA	
19	Male	17	2	R. PVI	NA	NA	

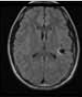

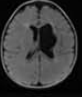
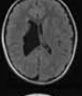
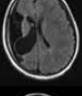
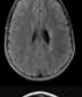
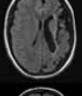
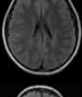

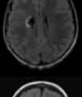
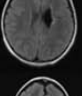
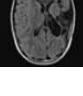
Case	Gender	Age at MR Imaging (yrs)	PSOM Motor	Stroke Type	AHA Motor	MA Motor	Image
20	Female	15	0	L. PT MCA	NA	NA	
21	Female	8	1	L. DM1 MCA	48	42	
23	Male	1	2	L. PVI	NA	NA	
24	Male	10	1	R. PVI	64	68	
27	Male	11	2	R. DM1 MCA	NA	NA	
28	Female	11	0.5	L. PVI	NA	NA	
29	Female	17	2	L. AT MCA	67	80	
31	Male	12	1	L. PVI	88	88	
32	Male	4	1	L. PVI	NA	NA	
33	Male	10	2	R. PVI	NA	NA	
34	Female	8	1	L. PVI	82	87	
35	Male	9	2	L. DM1 MCA	NA	NA	

Table 3.1. Patient demographics. Stroke types include middle cerebral artery (MCA) in the proximal M1 (PM1), distal M1 (DM1), posterior trunk (PT), or anterior trunk (AT), and periventricular infarction (PVI). PSOM score of 0 (normal), 0.5 (mild weakness with little impairment), 1 (moderate impairment), and 2 (severe impairment).

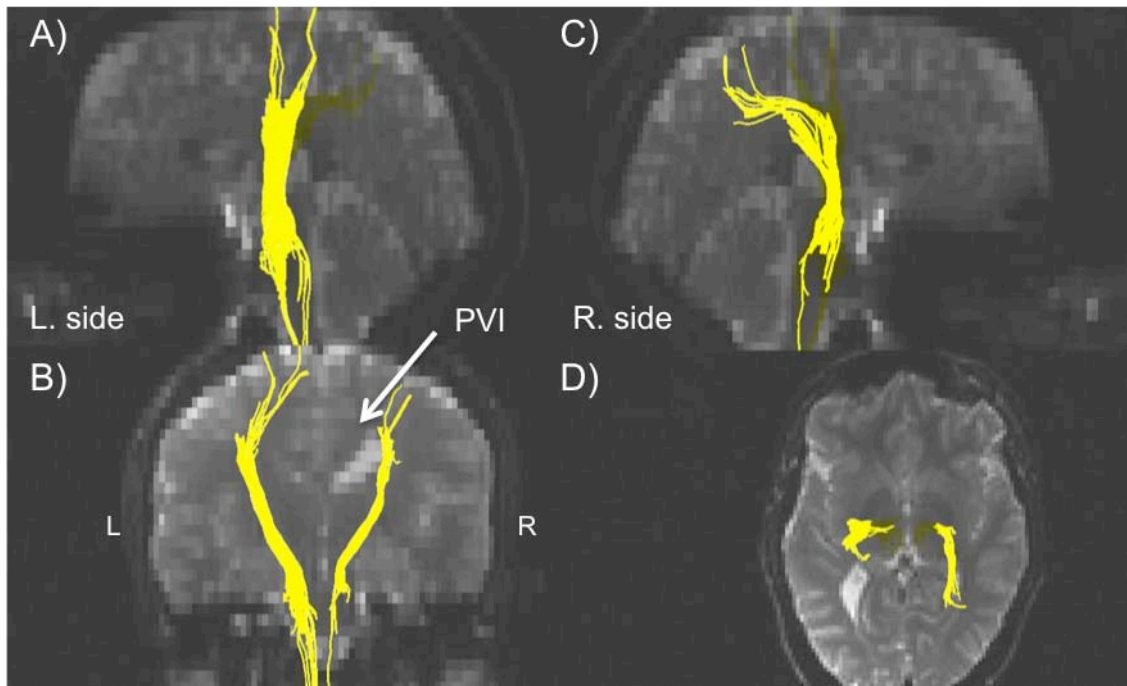


Figure 3.1. Example of lesioned and non-lesioned CST in a patient with a R. PVI. Healthy CST fibers (A), lesioned CST fibers (C), coronal view showing CST in both hemispheres (B) and lesion, and axial view (D).

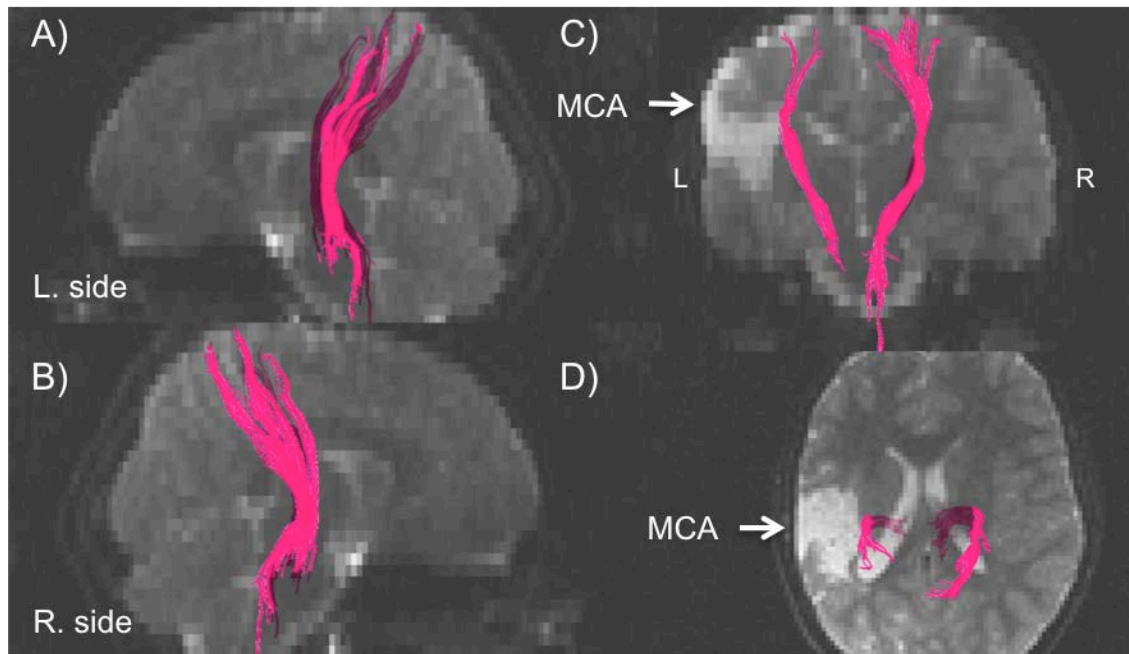


Figure 3.2. Example of lesioned and non-lesioned CST in a patient with a L. MCA. Lesioned CST fibers (A), healthy CST fibers (B), coronal view showing CST in both hemispheres (C) and lesion, and axial view (D).

3.1 Repeatability

Measurements for the repeatability analysis are presented in Tables 3.2 and 3.3. Good repeatability was found for all CST fiber counts ($ICC > 0.75$) (Table 3.2) and excellent repeatability was found for mean FA values in the full tract ($ICC = 0.98$).

Case	Healthy Fibers				Lesioned Fibers			
	Trial 1	Trial 2	Trial 3	Trial 4	Trial 1	Trial 2	Trial 3	Trial 4
1	128	126	132	115	14	15	10	4
2	115	198	206	114	5	5	5	12
3	108	113	103	126	21	22	21	34
4	135	207	209	142	73	80	70	46
7	112	120	109	104	68	94	71	23
8	29	53	53	40	25	6	16	18
11	372	305	328	231	67	53	42	34
12	77	80	74	43	7	9	6	10
13	115	132	90	79	13	14	13	14
14	60	76	62	64	15	13	16	16
17	74	94	91	61	36	39	39	12
ICC 0.91				ICC 0.76				

Table 3.2 Repeatability analysis for healthy and lesioned CST fiber counts in the full tract. Intraclass correlation (ICC) reported for 4 trials.

Case	Healthy Fibers				Lesioned Fibers			
	Trial 1	Trial 2	Trial 3	Trial 4	Trial 1	Trial 2	Trial 3	Trial 4
1	0.63	0.63	0.63	0.63	0.57	0.58	0.56	0.51
2	0.65	0.66	0.66	0.65	0.57	0.57	0.57	0.55
3	0.64	0.64	0.64	0.64	0.62	0.63	0.63	0.64
4	0.66	0.66	0.66	0.66	0.67	0.66	0.67	0.68
7	0.60	0.61	0.61	0.60	0.62	0.58	0.62	0.59
8	0.59	0.59	0.59	0.60	0.45	0.45	0.44	0.45
11	0.64	0.64	0.65	0.64	0.62	0.62	0.62	0.64
12	0.56	0.56	0.54	0.53	0.38	0.37	0.37	0.38
13	0.66	0.66	0.67	0.67	0.64	0.64	0.64	0.64
14	0.64	0.64	0.65	0.64	0.59	0.60	0.59	0.60
17	0.59	0.60	0.59	0.60	0.42	0.42	0.42	0.41
ICC 0.98				ICC 0.98				

Table 3.3. Repeatability analyses for healthy and lesioned CST mean FA in the full tract. Intraclass correlation (ICC) reported for 4 trials.

3.2 Aim 1 –Quantify and Compare the Diffusion Parameters between the Lesioned and Non-lesioned CST in Children with Perinatal Stroke

3.2.1 Fractional Anisotropy (FA)

Compared to the opposite side, FA was significantly decreased in the lesioned CST in all tract segments ($p < 0.01$) (Figure 3.3). From non-lesioned to lesioned CST there was a decrease of 0.03 (95% CI, -0.05 to -0.01) in the FT, 0.04 (95% CI, [-0.07 to -0.02]) in the UT, 0.11 (95% CI, [-0.15 to -0.07]) in the PT, 0.12 (95% CI, [-0.17 to -0.08]) in the MT, and 0.14 (95% CI, [-0.17 to -0.10]) in the ROI segment. The greatest difference was observed in the ROI segment ($p < 0.001$) though these measurements also had the largest overall variance.

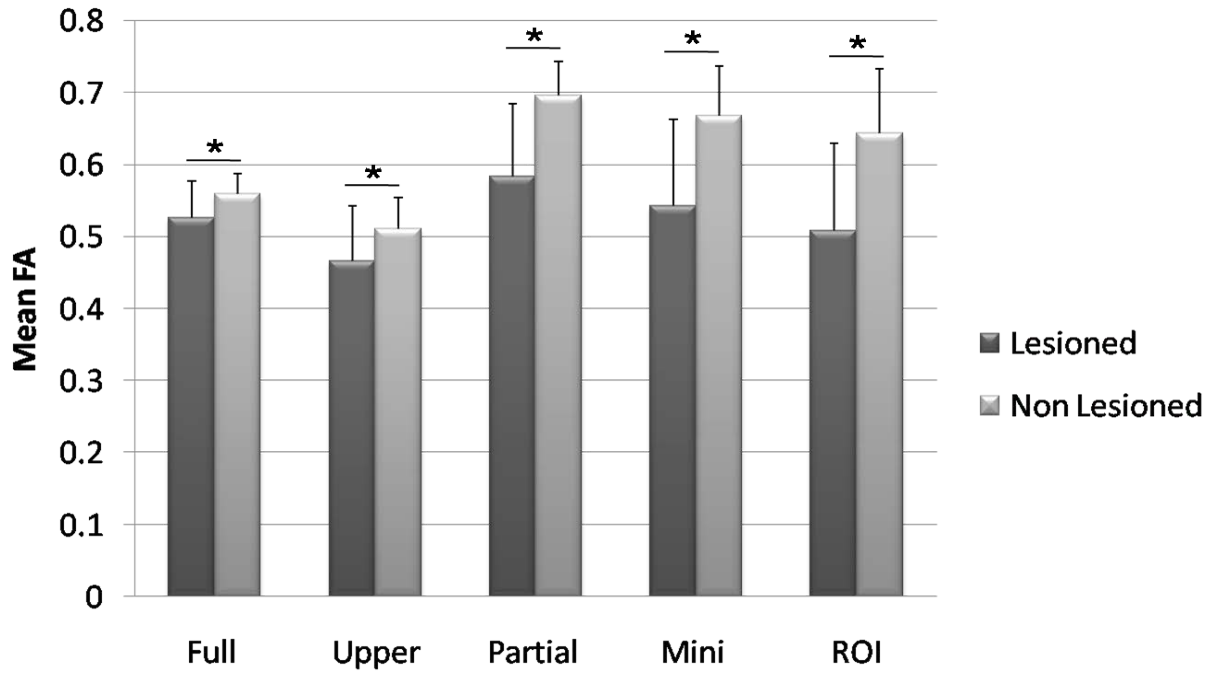


Figure 3.3. Mean FA values for lesioned versus non-lesioned CST across tract segments. n = 26 for full, 22 for upper, 23 for partial, 26 for mini, and 25 for ROI.

3.2.2 Axial Diffusivity (AD)

AD differences between the lesioned and non-lesioned sides were highly variable. The direction differed across tract measurement method. An increase was observed in the mean AD of the lesioned CST in the FT (0.09, 95% CI, 0.05 to 0.13 x 10⁻³ mm²s⁻¹, $p < 0.001$) and the UT (0.12, 95% CI, 0.03 to 0.21 x 10⁻³ mm²s⁻¹, $p = 0.01$). In contrast, the PT (0.05, 95% CI, -0.10 to 0.001 x 10⁻³ mm²s⁻¹) and the MT (0.13, 95% CI, -0.20 to -0.07 x 10⁻³ mm²s⁻¹) the mean AD was significantly decreased the in lesioned CST ($p < 0.04$). No difference was observed in the ROI segment for mean AD ($p = 0.825$) (Figure 3.4).

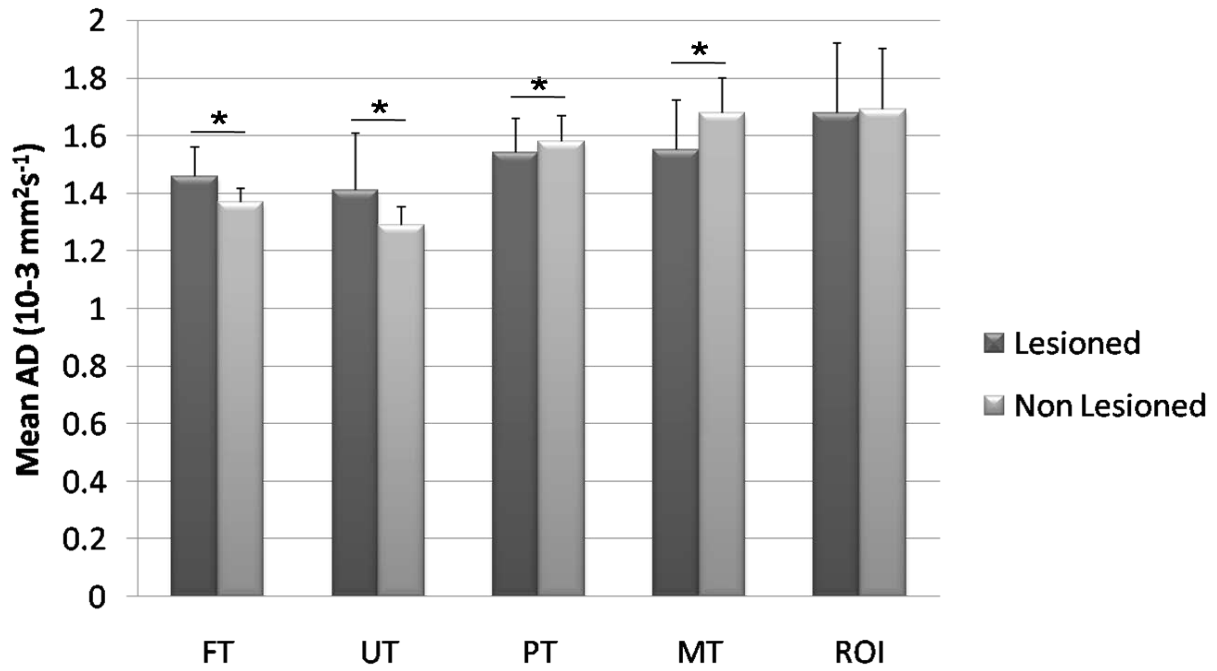


Figure 3.4. Mean AD values for lesioned versus non-lesioned CST across tract segments. n = 26 for full, 21 for upper, 23 for partial, 24 for mini, and 26 for ROI.

3.2.3 Radial Diffusivity (RD)

As seen in Figure 3.5, RD was significantly increased in the lesioned CST in all tract segments ($p < 0.001$). Mean RD increases from the non-lesioned to the lesioned CST were 0.07, (95% CI, 0.05 to 0.10 x 10⁻³ mm²s⁻¹) in the FT, 0.08 (95% CI, 0.04 to 0.13 x 10⁻³ mm²s⁻¹) in the UT, 0.13 (95% CI, 0.09 to 0.18 x 10⁻³ mm²s⁻¹) in the PT, 0.15 (95% CI, 0.09 to 0.20 x 10⁻³ mm²s⁻¹) in the MT, and 0.19 (95% CI, 0.13 to 0.26 x 10⁻³ mm²s⁻¹) in the ROI segment, were seen in the lesioned CST. The greatest difference was observed in the ROI segment though this again demonstrated the highest overall variance.

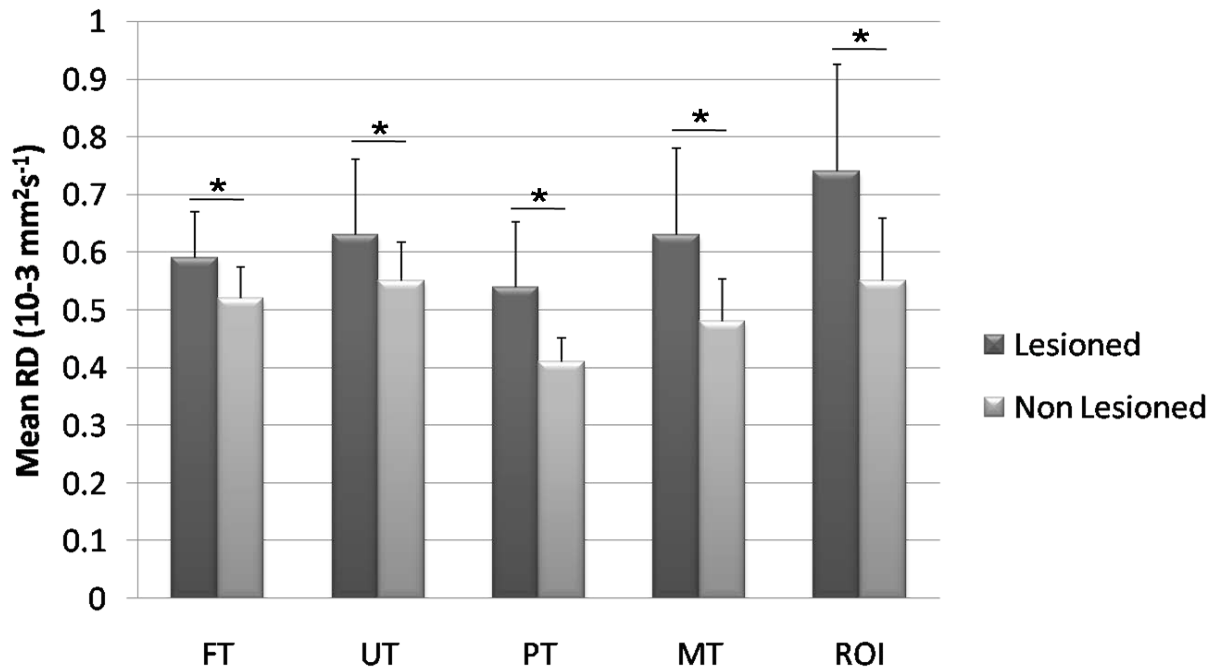


Figure 3.5. Mean RD values for lesioned versus non-lesioned CST across tract segments. n = 25 for full, 20 for upper, 23 for partial, 26 for mini, and 26 for ROI.

3.2.4 Mean Diffusivity (MD)

Mean MD was significantly increased in the lesioned CST compared to the non-lesioned in all of the tract segments ($p < 0.005$) (Figure 3.6). Increases were as follows: FT showed an increase of 0.09 (95% CI, 0.05 to 0.12 x 10⁻³ mm²s⁻¹), UT an increase of 0.07 (95% CI, 0.03 to 0.11 x 10⁻³ mm²s⁻¹), PT an increase of 0.07 (95% CI, 0.04 to 0.10 x 10⁻³ mm²s⁻¹), MT an increase of 0.05 (95% CI, 0.02 to 0.09 x 10⁻³ mm²s⁻¹), and the ROI segment showed an increase of 0.14 (95% CI, 0.07 to 0.20 x 10⁻³ mm²s⁻¹). The greatest difference and largest variance were observed in the ROI segment.

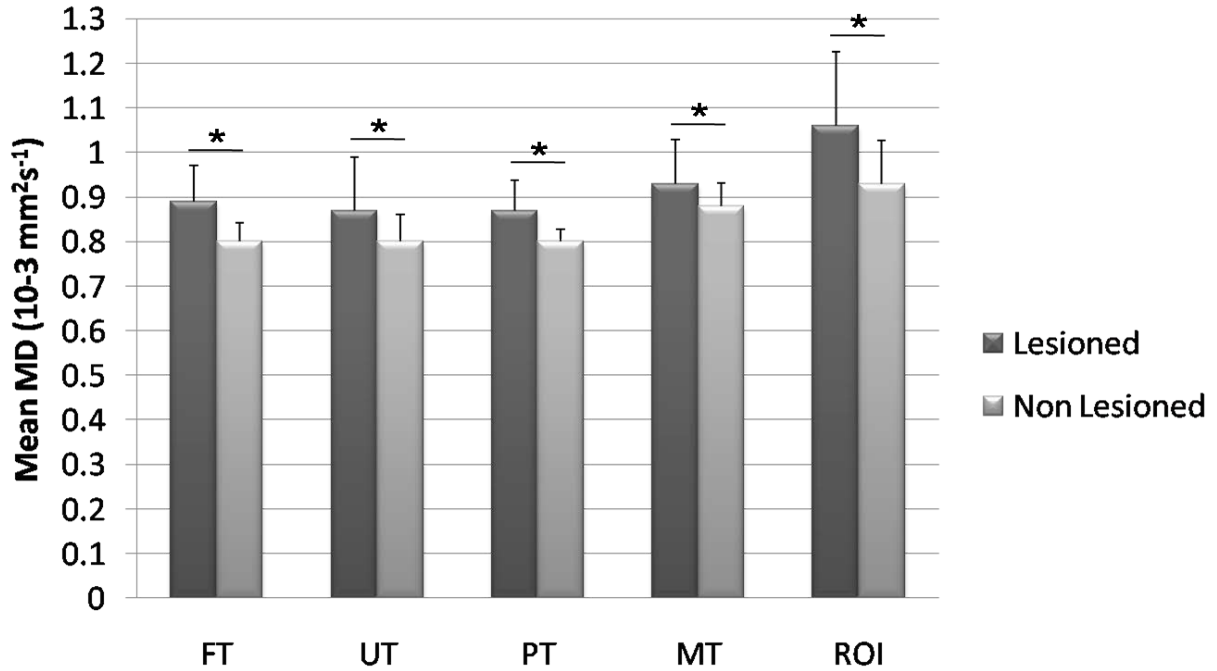


Figure 3.6. Mean MD values for lesioned versus non-lesioned CST across tract segments. n = 26 for full, 19 for upper, 23 for partial, 25 for mini, and 26 for ROI.

3.3 Aim 2 – Compare Diffusion Parameters within Different Segments of the CST

3.3.1 Fractional Anisotropy (FA)

FA symmetry decreased from FT (0.94 ± 0.09), to UT (0.91 ± 0.12), to PT (0.84 ± 0.14), to MT (0.81 ± 0.16), to cross-sectional ROI (0.77 ± 0.15). Mean FA symmetry was significantly different between the tract segments, $p < 0.001$. The degree of symmetry decreased steadily as the size of the tract decreased. The symmetry in the FT was significantly greater than the PT ($p = 0.028$), the MT ($p = 0.010$), and the ROI ($p < 0.001$). Further, the symmetry decrease from the UT to the ROI was also statistically significant ($p = 0.009$). There were no significant differences in FA symmetry between the rest of the tract segment combinations ($p > 0.05$) (Figure 3.7).

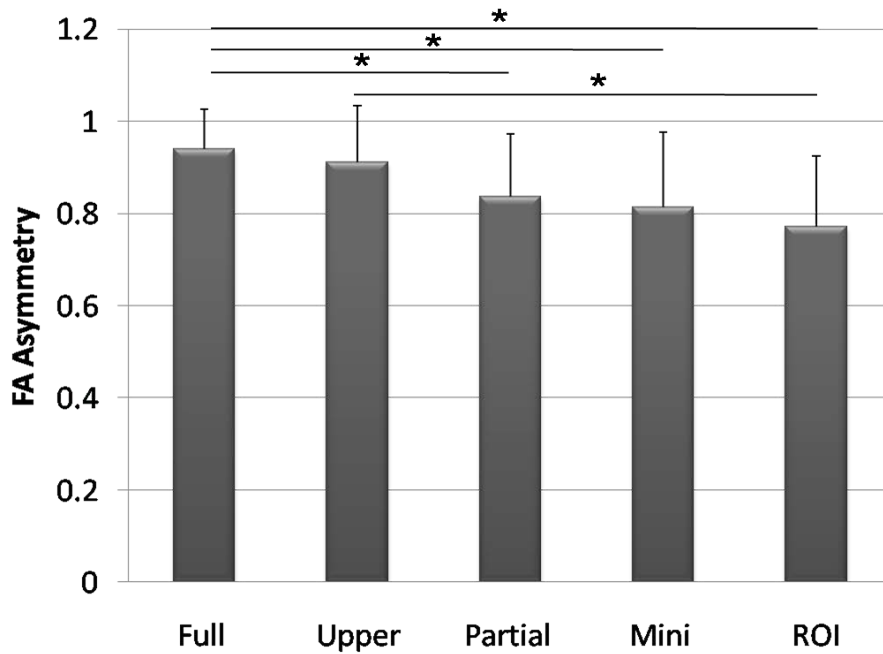


Figure 3.7. FA asymmetry across all tract segments. n = 26 in full, mini and ROI. n = 22 in upper and 23 for partial.

3.3.2 Axial Diffusivity (AD)

Compared to the other diffusion variables, AD showed the most consistent degree of symmetry.

FA, RD, and MD showed deviations of at least 0.20 (i.e. ratios 0.8 or 1.2) in one tract while AD values never deviated more than 0.08 in any tract. AD was the most symmetric in the ROI

segment (1.00 ± 0.13) followed by the partial (0.96 ± 0.06), full (1.07 ± 0.08), upper ($1.08 \pm$

0.15) and mini (0.92 ± 0.09). Mean AD symmetry was significantly different between the tract

segments, $p < 0.001$. Games-Howell post-hoc analysis revealed that the symmetry difference

between the FT and the PT and MT was significant ($p < 0.001$), as well as, the UT AD symmetry

was significantly different from the PT and MT ($p < 0.02$). No other significant AD differences

were seen between the tract segments (Figure 3.8).

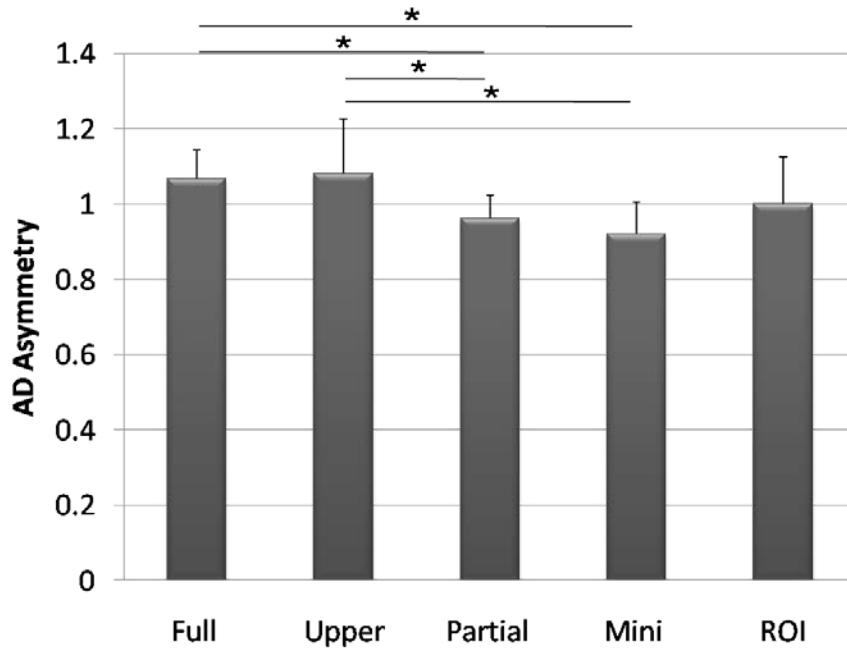


Figure 3.8. AD symmetry across all tract segments. n = 26 in full and ROI, n = 21 in upper, 23 in partial, and 24 in mini.

3.3.3 Radial Diffusivity (RD)

RD symmetry ratios demonstrated a decreasing trend as tract sizes diminished (Figure 3.7). RD symmetry decreased from the FT (1.14 ± 0.14) to the UT (1.15 ± 0.18) to the PT (1.33 ± 0.26). It then increased in the MT (1.32 ± 0.30) and the decreased again in the cross-sectional ROI analysis (1.37 ± 0.33). Mean RD symmetry was significantly different between the tract segments, $p = 0.001$. Games-Howell post-hoc analysis revealed a significant decrease in RD symmetry between the FT and the partial and ROI segment ($p < 0.04$). No other significant RD differences were seen between the tract segments (Figure 3.9).

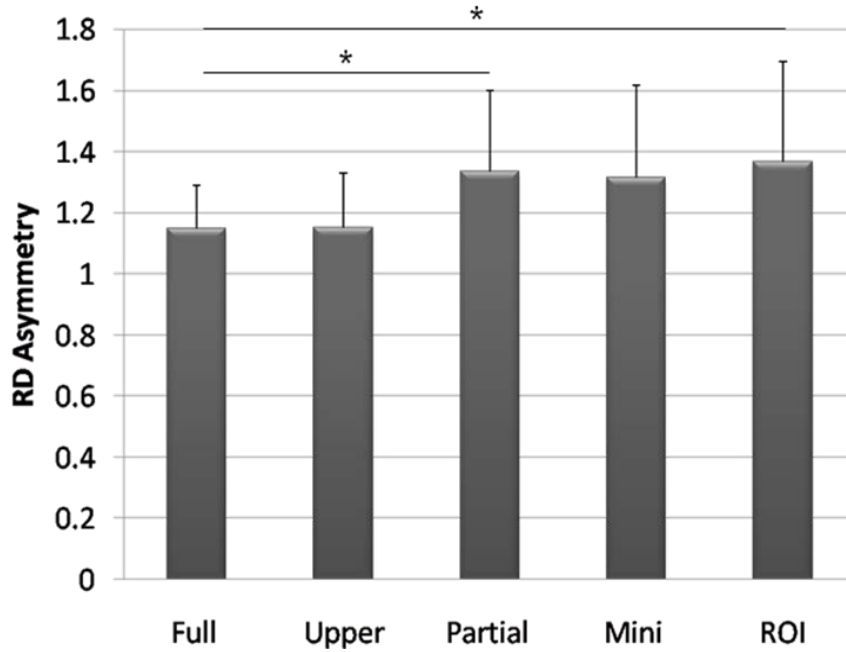


Figure 3.9. RD symmetry across all tract segments. n = 25 in full, 20 in upper, 23 in partial, 26 in mini and ROI.

3.3.4 Mean Diffusivity (MD)

MD symmetry demonstrated the greatest consistency across each tract segment. The ROI segment showed the least MD symmetry (1.15 ± 0.17) followed by the full (1.11 ± 0.10) and upper (1.11 ± 0.14) segments, with the partial (1.09 ± 0.09) and mini (1.06 ± 0.10) segments showing the most. Mean MD symmetry was not significantly different between the tract segments, $p = 0.159$ (Figure 3.10).

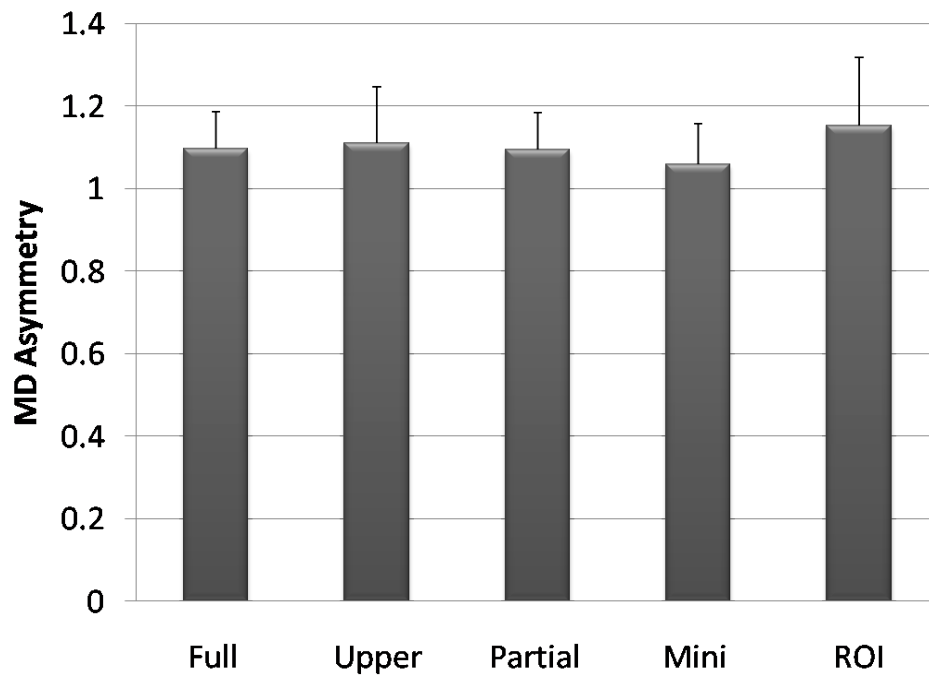


Figure 3.10. MD symmetry across all tract segments. n = 26 in full and ROI, 19 in upper, 23 in partial, and 25 in mini.

3.4 Mean Area Analysis of the Ventral Midbrain and Correlation with Motor Outcome

Mean cerebral peduncle area on the lesioned side (1.17 ± 0.35) was decreased compared to the non-lesioned side (1.58 ± 0.25), a significant decrease of 0.41 (95% CI, -0.54 to -0.27) cm^2 , $p < 0.001$ (Figure 3.11). There was a significant association between cerebral peduncle area and motor outcome (PSOM) with cerebral peduncle symmetry decreased in the severe outcome group (Figure 3.12). The degree of symmetry also correlated with AHA and MA outcome scores with decreased symmetry correlating with worse outcome (Figure 3.13).

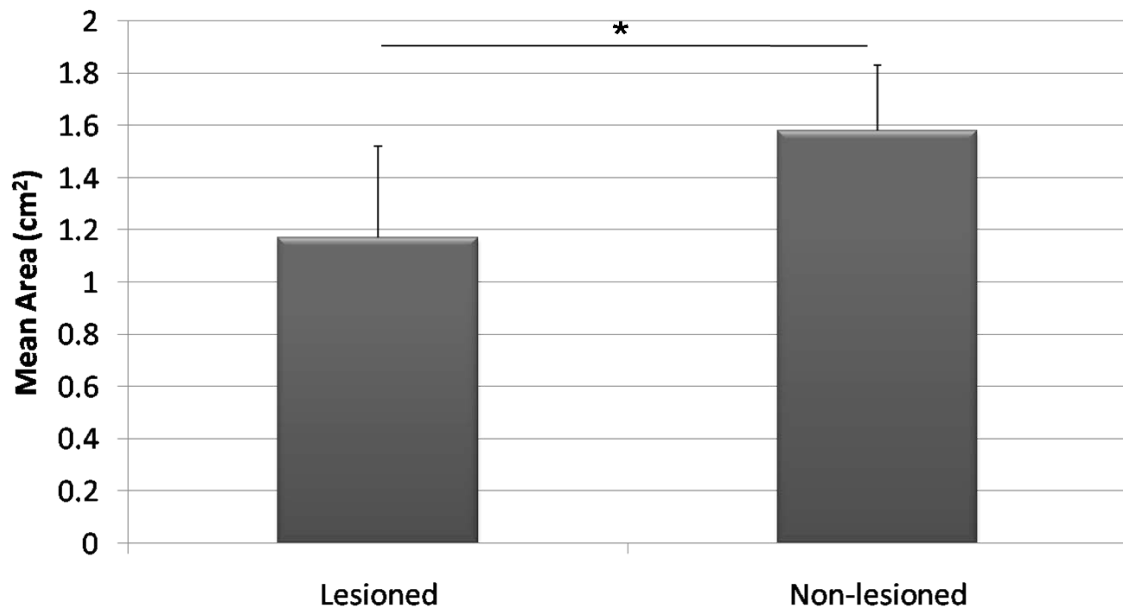


Figure 3.11. Ventral midbrain mean area calculations of the lesioned and non-lesioned CST. n = 26.

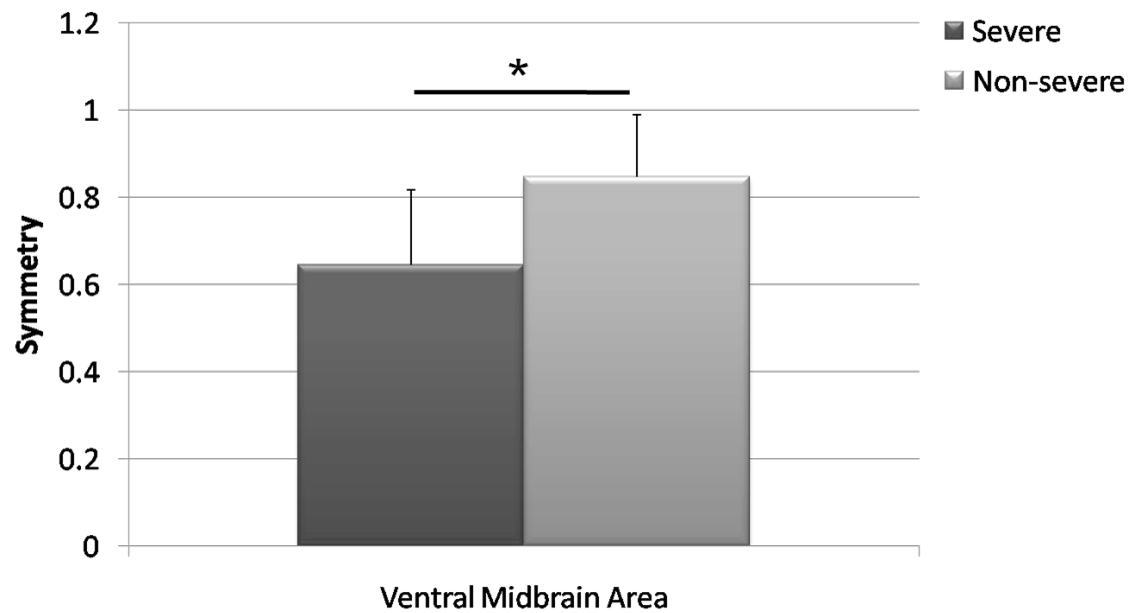


Figure 3.12. Ventral midbrain mean area symmetry across severe (PSOM = 2) and non-severe motor outcome (PSOM = 0-1), n = 26.

*** p < 0.05.**

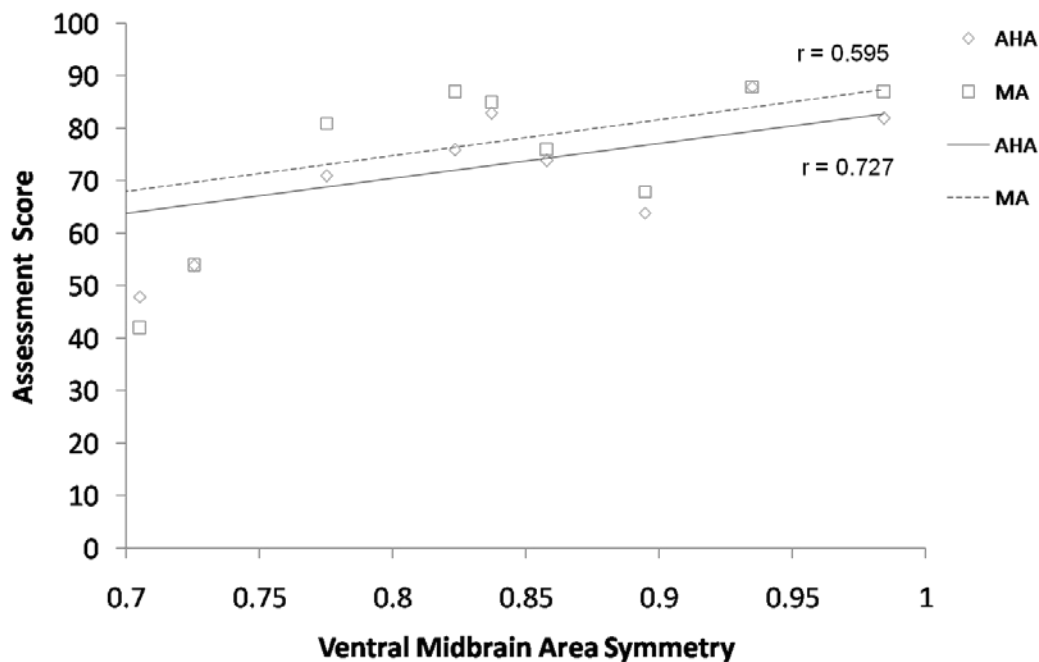


Figure 3.13. The relationship between motor assessment score (AHA and MA) and ventral midbrain area symmetry, $n = 16$.

3.5 Aim 3 – Determine Associations between the CST Diffusion Measures and Motor Outcome

3.5.1 Diffusion Symmetry Associations with PSOM severity

In the full tract segment, FA symmetry was the only variable associated with PSOM outcome group and the strength of association was weak. FA symmetry was decreased in the severe motor outcome group (0.91 ± 0.08) compared to the non-severe group (0.97 ± 0.05) a significant difference 0.06 (95% CI, 0.002 to 0.115), $p = 0.043$. The remaining diffusion variables - AD, RD, and MD mean symmetry scores did not differ between the non-severe and severe motor outcome groups, $p > 0.05$ (Figure 3.14).

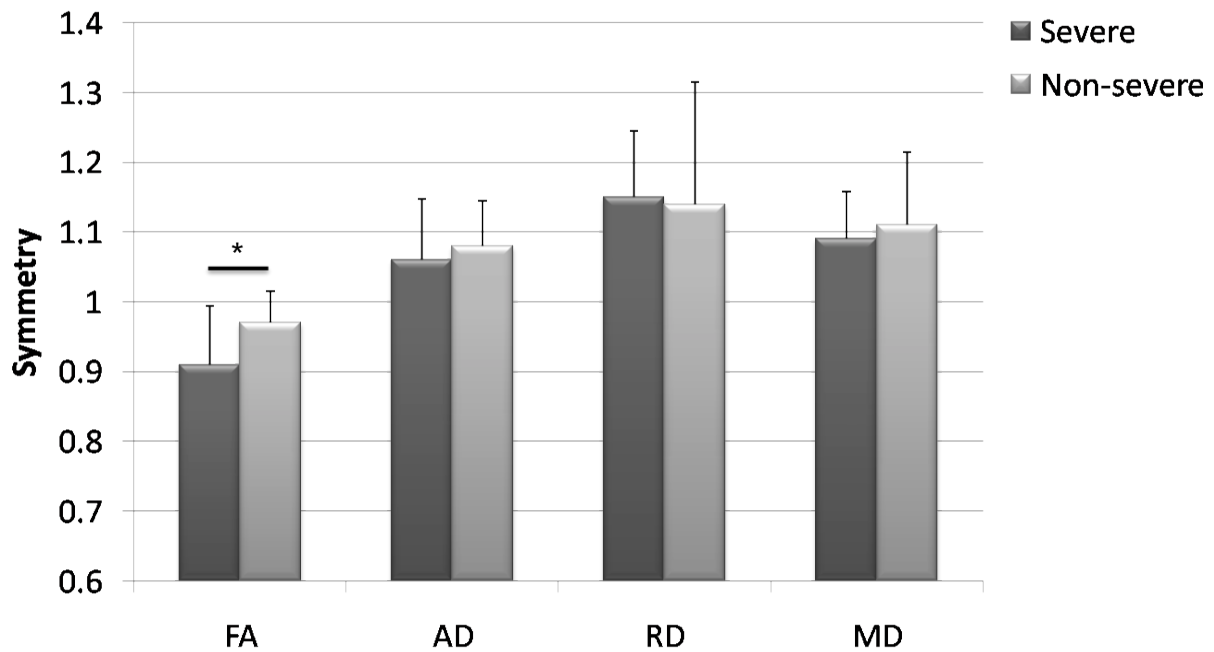


Figure 3.14. Full tract diffusion variables across severe and non-severe motor outcome, n = 24 in FA, 26 in AD, and 25 in RD and MD.

The partial tract demonstrated a significant association between multiple diffusion variables and PSOM motor outcome. FA symmetry was decreased in the severe motor outcome group (0.76 ± 0.11) compared to the non-severe motor outcome group (0.91 ± 0.11) a difference of 0.15 (95% CI, 0.06 to 0.25), $p = 0.003$. AD symmetry was decreased in the severe motor outcome group (0.93 ± 0.05) compared to the non-severe motor outcome group (0.99 ± 0.06), a difference of 0.06 (95% CI, 0.013 to 0.110), $p = 0.015$. RD and MD mean symmetry scores did not differ between motor outcomes, $p > 0.05$ (Figure 3.15).

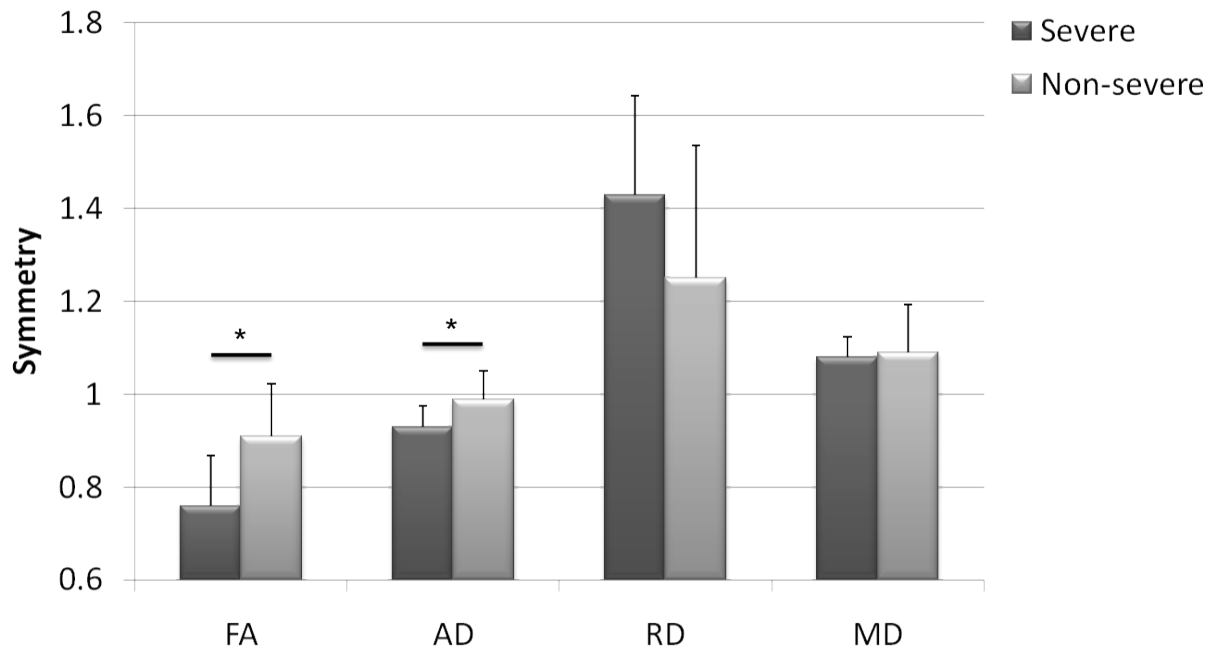


Figure 3.15. Partial tract diffusion variable symmetries across severe and non-severe motor outcome, n = 26 in FA and RD and 25 in AD and MD.

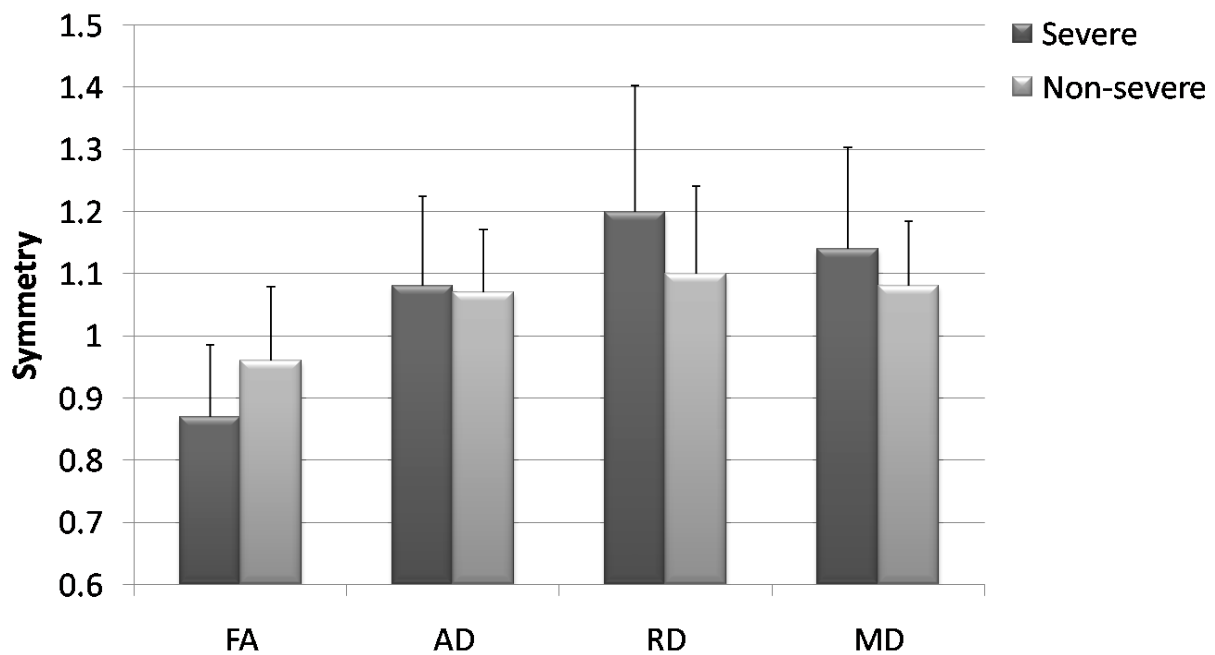


Figure 3.16. Upper tract diffusion variable symmetries across severe and non-severe motor outcome, n = 22 in FA, 20 in AD, RD, and MD.

In a similar fashion to PT, several MT variables correlated with PSOM outcomes. FA symmetry was decreased in the severe motor outcome group (0.74 ± 0.11) compared to the non-severe motor outcome group (0.88 ± 0.18) a significant difference of 0.14 (95% CI, 0.18 to 0.26), $p = 0.027$. AD symmetry was also associated with PSOM severity in the mini tract, being decreased in the severe motor outcome group (0.87 ± 0.07) compared to the non-severe motor outcome group (1.00 ± 0.11) a difference of 0.13 (95% CI, 0.05 to 0.20), $p = 0.002$. The remaining variables RD and MD mean symmetry scores did not differ between motor outcome groups, $p > 0.05$ (Figure 3.17). There were no significant differences between PSOM motor outcomes groups for any diffusion variable in either the UT or cross-sectional ROI analysis (Figure 3.16 and 3.18).

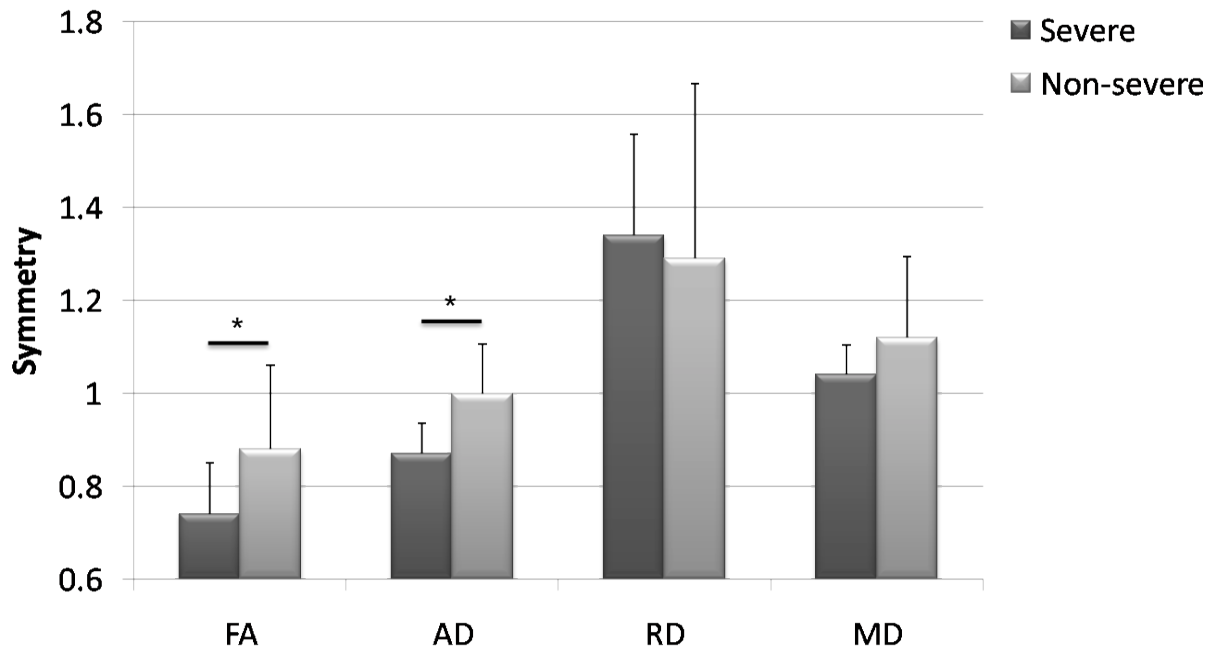


Figure 3.17. Mini tract diffusion variable symmetries across severe and non-severe motor outcome, n = 26 in FA, RD and MD, and 25 in AD.

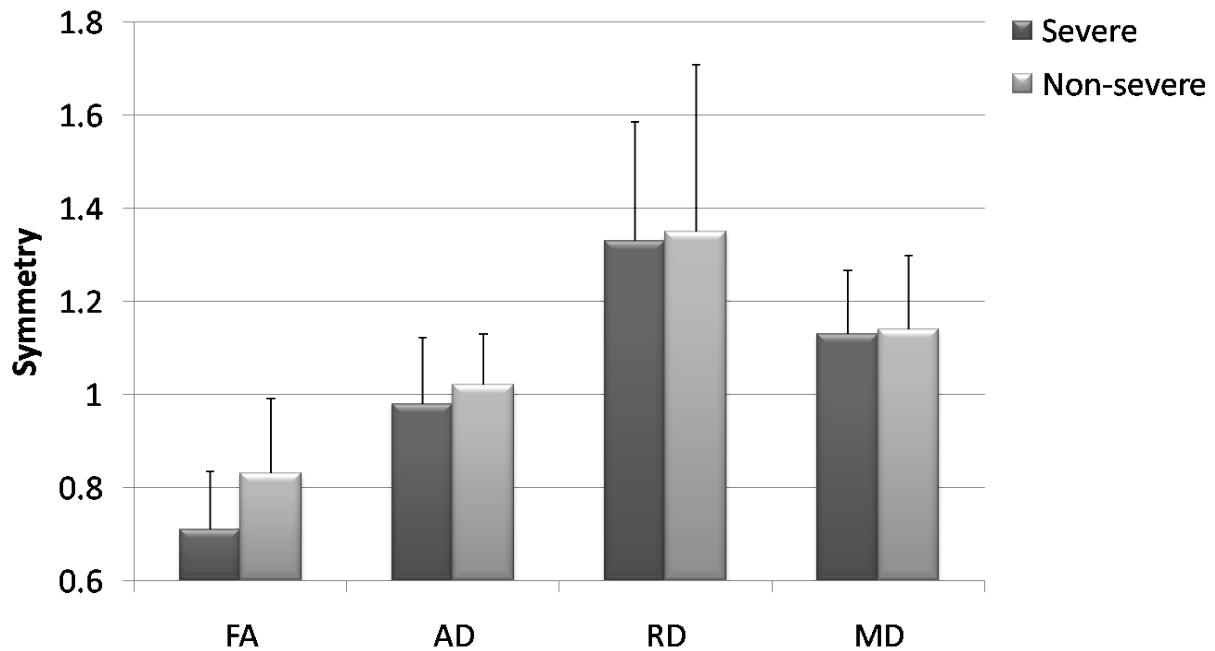


Figure 3.18. Cross-section ROI analysis diffusion variable symmetries across severe and non-severe motor outcome.

Therefore, based on the dichotomized outcome of severe versus non-severe motor dysfunction according to the PSOM, FA and AD in the PT and MT segments were the only diffusion variables to demonstrate a significant difference between good and poor motor outcome.

However, AD, had the most inconsistent symmetry established in the side to side comparisons (see section 3.2 above).

3.5.2 Diffusion Symmetry Correlations with AHA and MA Motor Scores

Correlations between different diffusion variables across each tract method for the AHA and MA are summarized in Table 3.4. The UT was the only measure that showed consistent correlations across all diffusion variables for both the AHA and MA motor measures ($p < 0.024$) (Figure

3.19). The FT and PT also showed consistent strong correlations to motor outcomes with most diffusion variables ($p < 0.018$), the exceptions being the AD in the PT and FA in the FT. Finally, only FA symmetry demonstrated consistent correlations with AHA and MA motor outcomes in both MT ($p = 0.002$) and cross-section ROI analysis ($p < 0.024$).

In summary, the UT shows the most consistent correlation between diffusion variable and motor outcome, followed closely by the partial and full tracts. Within these 3 tract segments, RD and MD symmetry were consistently and strongly correlated with both motor outcome measures, while FA (the most commonly investigated diffusion variable) was significantly correlated in all segments except the FT.

Tract	Variable	AHA score	Melbourne score
		Pearson correlation (sig. 2 tailed)	Pearson correlation (sig. 2 tailed)
Full	FA	0.362 (0.168)	0.479 (0.061)
	AD	-0.615 (0.011)*	-0.689 (0.003)*
	RD	-0.655 (0.006)*	-0.729 (0.001)*
	MD	-0.674 (0.004)*	-0.750 (0.001)*
Upper	FA	0.830 (0.001)*	0.940 (< 0.001)*
	AD	-0.644 (0.024)*	-0.754 (0.005)*
	RD	-0.862 (< 0.001)*	-0.951 (< 0.001)*
	MD	-0.799 (0.002)*	-0.909 (< 0.001)*
Partial	FA	0.757 (0.003)*	0.821 (0.001)*
	AD	0.424 (0.149)	0.391 (0.186)
	RD	-0.674 (0.012)*	-0.791 (0.001)*
	MD	-0.641 (0.018)*	-0.722 (0.005)*
Mini	FA	0.662 (0.005)*	0.705 (0.002)*
	AD	0.724 (0.002)*	0.701 (0.002)*
	RD	-0.268 (0.316)	-0.358 (0.174)
	MD	0.212 (0.431)	0.172 (0.523)
ROI	FA	0.823 (< 0.001)*	0.807 (< 0.001)*
	AD	0.344 (0.192)	0.270 (0.313)
	RD	-0.561 (0.024)*	-0.622 (0.010)*
	MD	-0.032 (0.905)	-0.81 (0.766)

Table 3.4. Correlation of diffusion variable SI for each tract with AHA and MA Motor Score. *Significant correlation

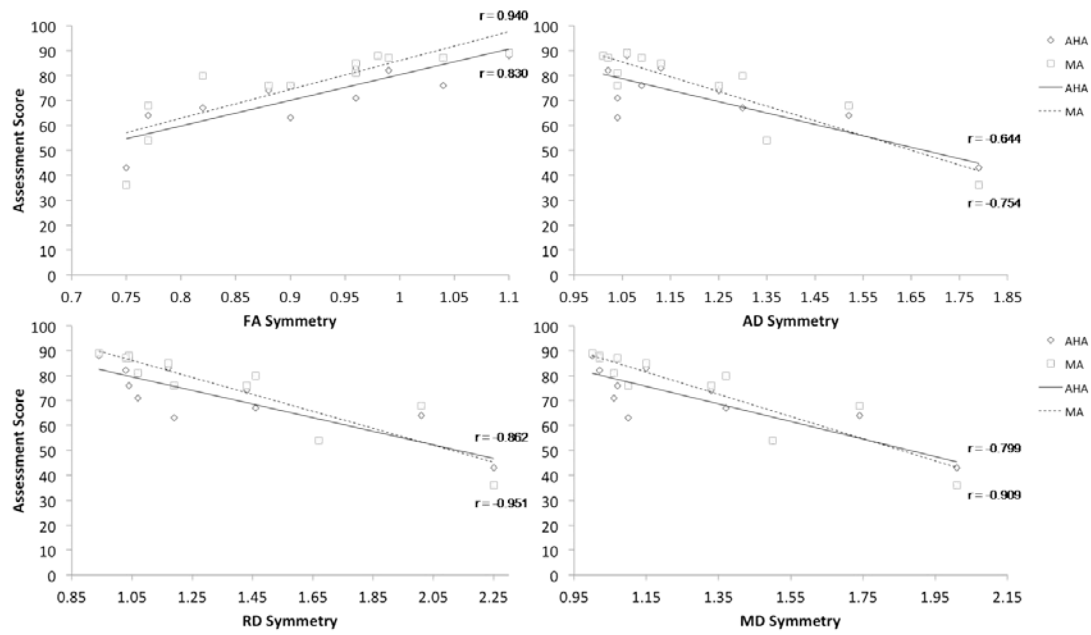


Figure 3.19. The relationship between motor assessment score (AHA and MA) and inter-hemispheric symmetry of CST diffusion in the upper tract, n = 16.

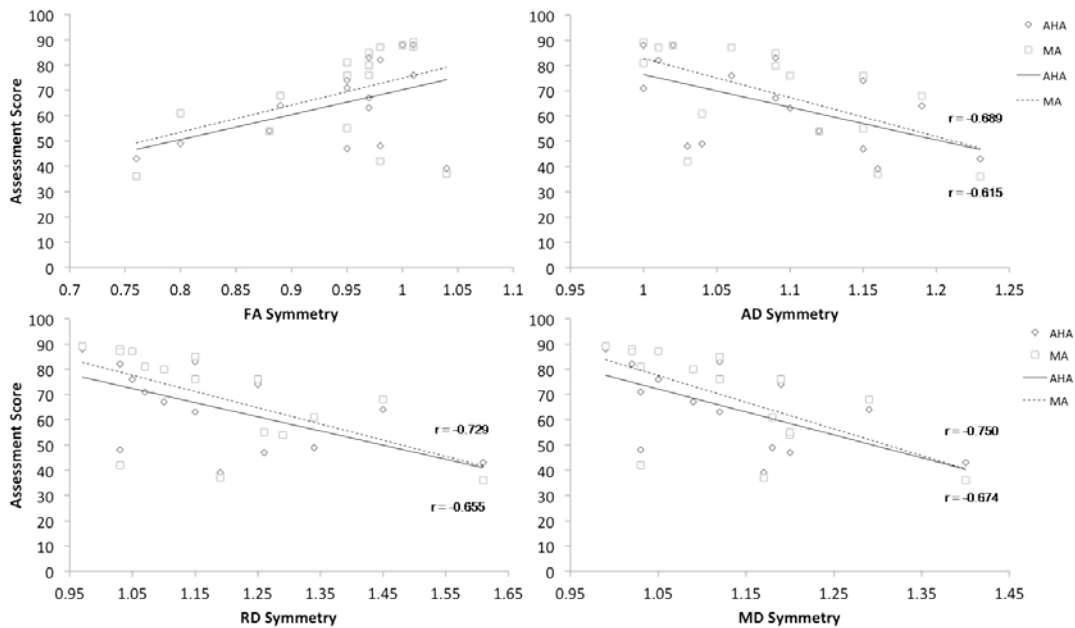


Figure 3.20. The relationship between motor assessment score (AHA and MA) and inter-hemispheric symmetry of CST diffusion in the full tract, n = 16.

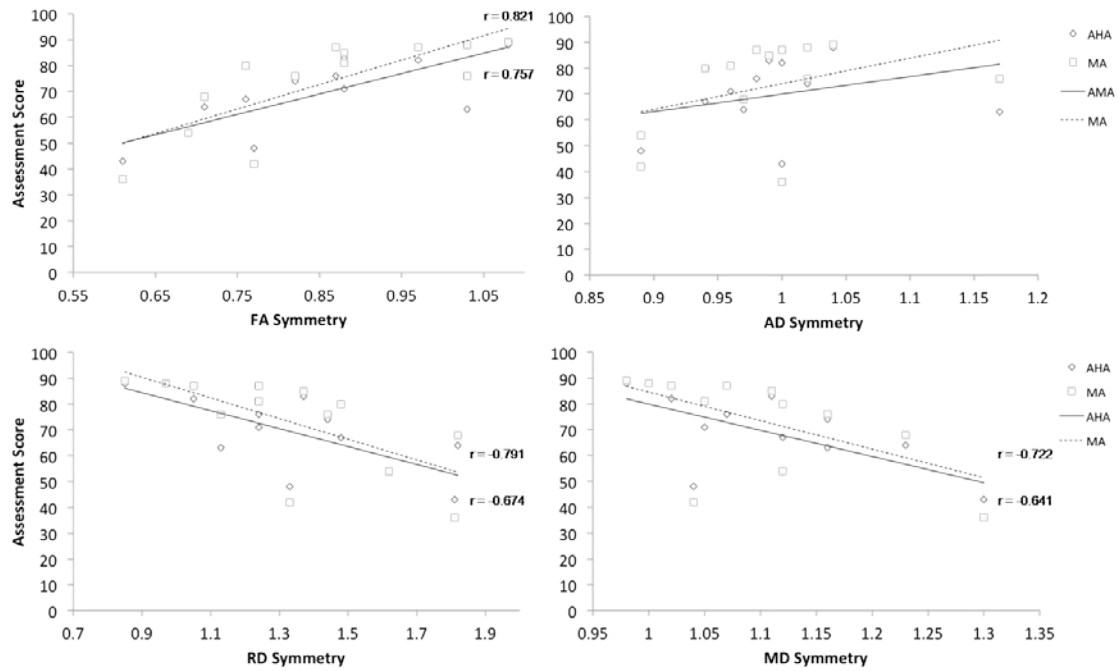


Figure 3.21. The relationship between motor assessment score (AHA and MA) and inter-hemispheric symmetry of CST diffusion in the partial tract, n = 16.

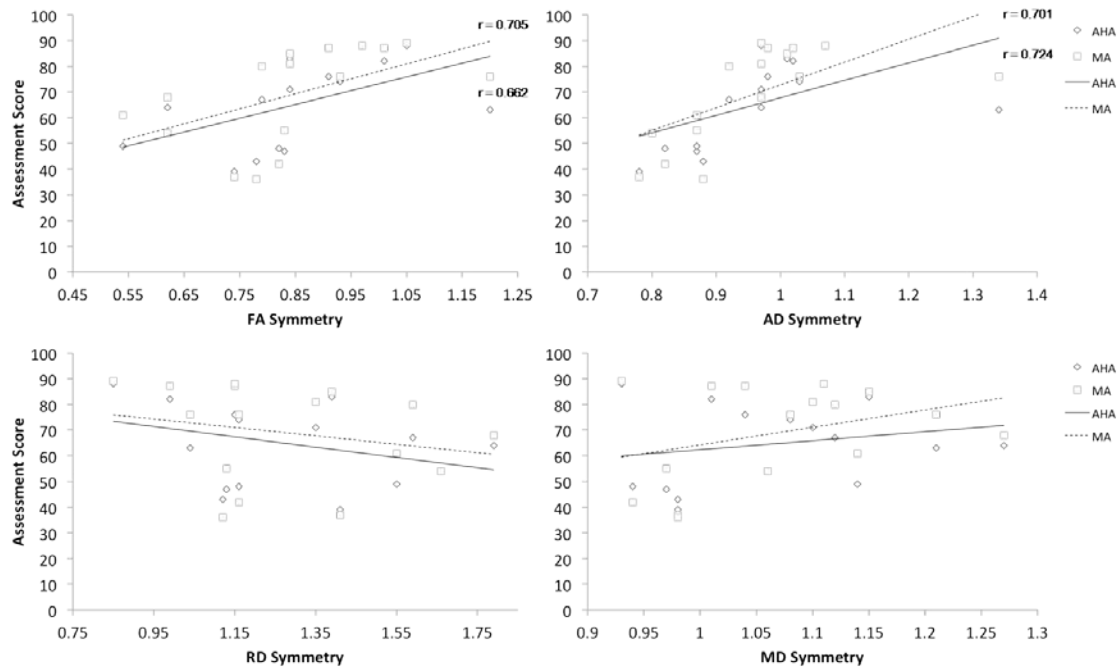


Figure 3.22. The relationship between motor assessment score (AHA and MA) and inter-hemispheric symmetry of CST diffusion in the mini tract, n = 16.

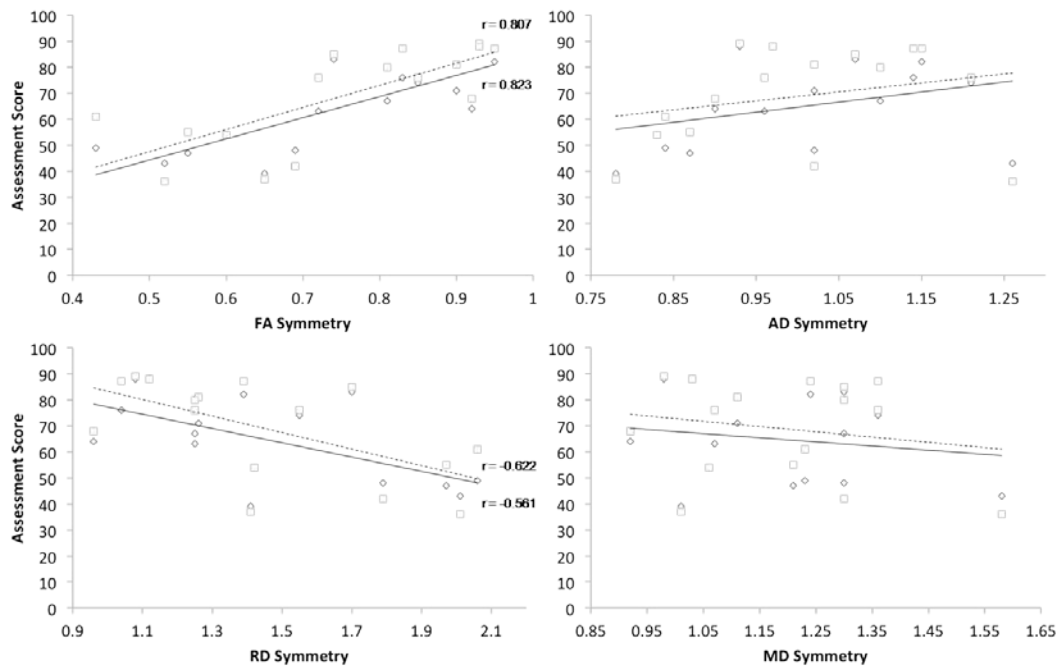


Figure 3.23. The relationship between motor assessment score (AHA and MA) and inter-hemispheric symmetry of CST diffusion in the cross section ROI analysis, n = 16.

3.6 Outliers, Normality, and Homogeneity of Variances

Outliers were assessed using the difference scores between lesioned and non-lesioned diffusion variables for the paired samples t-test, the ratio scores for the ANOVA, and the group means for the independent t-tests. Any outlier greater than two standard deviations from the mean was considered extreme. All such data points were double checked for accuracy including repeat measurement. Once confirmed, extreme outliers were removed from the respective sample. The number of outliers removed across each analysis performed was small with counts summarized in Table 3.5. Based on common practice any outlier greater than 2 standard deviations from the mean was deemed to be extreme. Extreme outliers were removed in the paired Samples t-tests, ANOVA, and independent t-tests (Table 3.5).

Normality was assessed using the Shapiro-Wilks test. While no variable had clearly non-normal distribution, formal testing revealed mixed results for normality across different variables and tract segments. For the paired t-test analysis, several variables failed the test for normality including FA in the ROI segment; RD in the upper tract, and MD in the full and upper tracts, in these cases the non-parametric Wilcoxon Signed-Ranks Test was performed. Comparable results were found between the non-parametric (Wilcoxon Signed-Rank test) and the original parametric test (paired-samples t-test) and did not alter any of the conclusions reached above.

In the ANOVA analysis, MD was not normally distributed in 3 of the tracts, and the RD was not normally distributed in one so an additional non-parametric Kruskal-Wallis H test was run. Regardless of statistical test (ANOVA or Kruskal-Wallis H) the results were comparable so we used the values from the ANOVA. Homogeneity of Variances was violated, as assessed by Levene's Test of Equality of Variances, so the robust ANOVA test, the Welch's ANOVA and the Games-Howell post-hoc test were used.

For analysis across severe and non-severe outcome, the diffusion variables means were normally distributed with the exception of the non-severe FT RD, non-severe FA in the ROI, and severe UT FA, RD, and MD. In these few cases an additional non-parametric Mann-Whitney U statistical test was performed. Comparable results were found so we again chose to use the results from the independent samples t-test for this section. If homogeneity of variances was violated, as assessed by the Levene's Test for Equality of Variances, separate variances and the Welch-Satterthwaite correction were used.

Tract	Variable	Paired t-test	Independent t-test	ANOVA
Full	FA	-	2	-
	AD	-	-	-
	RD	1	1	1
	MD	-	1	1
Upper	FA	-	-	-
	AD	1	2	2
	RD	2	2	2
	MD	1	2	2
Partial	FA	-	-	-
	AD	-	1	1
	RD	-	-	-
	MD	-	1	-
Mini	FA	-	-	-
	AD	-	1	2
	RD	-	-	-
	MD	1	-	1
ROI	FA	1	-	-
	AD	-	-	-
	RD	-	1	-
	MD	-	1	-

Table 3.5. Outliers were analysed and removed individually for each statistical test. Any outlier greater than 2 standard deviations from the mean was deemed extreme and removed.

CHAPTER 4 – DISCUSSION

In this study, we examined the integrity of the lesioned CST in 26 children following unilateral perinatal ischemic stroke. We successfully completed our primary aim by demonstrating the ability of DTI to quantify differences in CST integrity after perinatal stroke. We also provide novel data to suggest that strategic analysis of different CST segments may offer additional and relevant information over and above more traditional full tract or ROI approaches. We demonstrated consistent correlations between DTI parameters and well-characterized motor outcome measures supporting clinical relevance and utility of CST DTI in studies of neuroplasticity and interventional rehabilitation following perinatal stroke.

4. Comparison to Related Studies

Our results are generally consistent with the limited existing literature examining CST injury and integrity following perinatal stroke^{46,82}. Inter-hemispheric asymmetry was found for the diffusion variables FA and RD in all studies. One study found there were no asymmetries for any diffusion variables in the control group but there was increased asymmetry of FA, RD, and tract volume that were associated with motor dysfunction following neonatal ischemic or hemorrhagic stroke⁴⁶.

Another recent study explored the ability of DTI to predict long-term motor outcome very early after perinatal stroke (3 months)⁸². This study found increases in inter-hemispheric CST asymmetry for FA, RD, and ADC. Specifically, the decreases in lesioned CST FA found correlated with early motor outcomes at 18 months⁸². Unlike other studies^{57,58,82}, we found significant differences in AD between lesioned and non-lesioned CST (in most tract segments)

although as with the other studies, this difference did not consistently correlate with motor outcome. These findings are consistent with previous acute, clinically obtained diffusion weighted imaging of the CST which has demonstrated correlations with long-term motor outcomes in neonatal⁸³, childhood³⁰ and adult⁵ stroke. It remains unknown how well acute diffusion and DTI imaging correlate with the long-term chronic DTI abnormalities described here. More careful exploration of this relationship in the future might provide novel insight into how the CST matures during early development following perinatal stroke.

Our measurements of cerebral peduncle area comparisons are also consistent with previous volumetric anatomical studies of CST Wallerian degeneration in neonatal stroke, the degree of which correlates with motor outcome⁸³. We replicated these findings in the current study demonstrating that the degree of cerebral peduncle area symmetry correlates with motor outcome. Recent neonatal stroke animal evidence has correlated such Wallerian degeneration pathologically with CST diffusion imaging parameters³⁴. Combining our new DTI data with the above evidence from different populations, timing, imaging, and pathology provides an improved understanding of CST pathophysiology following perinatal stroke.

4.1 Quantification of Diffusion Variables in the CST

Using DTI, we quantified 4 commonly investigated diffusion parameters (FA, AD, RD, and MD) within the lesioned and non-lesioned CST in the chronic phase of perinatal stroke. Three of these diffusion variables (FA, RD, and MD) showed significant differences between the lesioned and non-lesioned CST regardless of measurement method (fiber tracking and cross sectional analysis). Further, these differences were consistent in the direction of asymmetry between the lesioned and non-lesioned CST. In contrast, AD did not exhibit a significant difference between

hemispheres with the ROI analysis and was inconsistent in the direction of asymmetry suggesting that AD is likely an unreliable diffusion parameter for investigating CST integrity in our population.

In contrast, the other diffusion variables seem to demonstrate potential utility in CST functional assessment. While FA describes the anisotropy within the tissue, MD characterizes the mean diffusion. Both are highly dependent on diffusion parallel and perpendicular within the tract. The decrease in anisotropy we found is most likely due to the increase in the radial diffusion. Previous studies report that decreased FA and increased RD are associated with a worse motor outcome following stroke. Similar patterns of diffusion have previously been reported within the CST in adult stroke^{64,77,80}, in children with congenital hemiparesis⁷⁸ (not stroke related), and in children with non-specific motor dysfunction⁵⁷. Consistent with these findings, our study demonstrated both a decrease in FA and increase in RD within the CST. This pattern might be explained by a decrease in axonal density and/or myelin density^{84,85}. A reduction in physical barriers to diffusion, such as, cellular membranes and myelin, would permit greater diffusion in the direction perpendicular to the tract. Studies in animal models have demonstrated that the presence of myelin is a component of anisotropy within white matter. Specifically, decreases in myelin resulting from genetic deficiencies result in increased RD and decreases in anisotropy⁸⁶. In line with the current study, rats exposed to hypoxic-ischemic conditions in utero resulting in hypertonia had reduced anisotropy (FA) with increased transverse diffusion in the PLIC⁸⁷. It is also possible that the number of axons in the lesioned CST is reduced compared to the non-lesioned CST, or that there is something structurally different with the axons themselves. While the exact intracellular and extracellular components that contribute to diffusion cannot be elucidated from the current study, our results provide *in vivo* evidence to

suggest altered integrity in the lesioned CST. We suggest that RD may provide the most accurate, clinically relevant diffusion parameter of CST integrity in perinatal stroke. Therefore, although FA has historically been the most common variable assessed, our results suggest that others like RD and MD carry a similar utility. Given that each provides different information about the physiological properties of the injured tract, we suggest that future studies should consider the inclusion and comparison of each.

4.2 The Non-lesioned CST

For the purposes of our study, the non-lesioned CST was assumed to be healthy and was used as an internal control. The main advantage of this approach is that each person serves as his or her own “internal control”. The expression of the diffusion variables as a ratio (lesioned/non-lesioned) allowed immediate correction of many potentially confounding factors including age, gender, genetics, and what are likely many other inter-individual differences in brain structure and neurophysiology. This approach has been used in many other DTI studies of the CST in both children and adults^{46,68,78,82}. However, there is evidence suggesting that the non-lesioned CST may not be entirely normal following stroke. A recent study in adult stroke reported reduced integrity (lower FA compared to controls) within the contralesional CST⁶⁸.

Furthermore, emerging models of developmental plasticity following perinatal stroke have established the importance of ipsilesional projections from the unlesioned hemisphere to the affected sides⁸ (see below). The degree that diffusion variables are affected in such modified CST pathways remains unknown in perinatal stroke. To address this issue, we are developing further studies that will investigate how the non-lesioned CST compares with a group of age-matched controls. We will also explore possible connections between the non-lesioned CST diffusion

parameters with brain stimulation parameters of CST integrity (transcranial magnetic stimulation, TMS) and motor control.

4.3 Fiber Tracking versus. Cross-sectional ROI Analysis

A major aim of our study was to determine if interrogations of different segments of the CST would provide advantages over traditional methods. Most previous DTI studies in stroke and cerebral palsy use one of two methods: full fiber tracking or two-dimensional ROI analysis). Fiber tracking is useful when the tract in question is intact (e.g., non-lesional diseases and normal child development studies). The main advantages of this method are that it uses a semi-automated approach, which minimizes user input, and can evaluate functional tracts in their entirety. However, several disadvantages include subjective components of which fibers are included in the tract and the resolution of crossing fibers. On the other hand, ROI analysis methods allow for specific anatomical localizations but are only two-dimensional, lacking the functional specificity afforded by tractography.

Investigations of CST integrity in adult stroke and congenital hemiplegia studies using both methods have successfully demonstrated associations between motor outcomes diffusion parameters^{68,88}. It has not been established which of these methods is superior as a gold standard for integrity quantification does not exist⁶² and no comparisons of different methods have been attempted in populations relevant to ours.

Our study is the first to our knowledge that generated and compared a spectrum of CST measures, ranging from full tracts to partial and mini tracts, and two-dimensional ROIs. As expected, we observed that methods requiring the most fiber tracking were increasingly difficult to obtain in children with large arterial strokes. The partial tract method was successful in

mitigating this as most patients with MCA lesions still had intact CST between the cerebral peduncle and PLIC. There were only a few cases where the lesions were so severe that the partial tract measurement was not possible leaving the mini tract and ROI options. This suggests a partial tract approach could be applicable to the majority of children with perinatal stroke.

Our study included a comparison of different analyses within the fiber tracking method itself. We hypothesized that a “compromise” between the full tractography and ROI approach might offer the best of both methods: the functional specificity of tractography without the added variance of the full tract while also being able to capture the children with large arterial lesions and limited CST available for analysis. We found that both methods can reliably map CST integrity in the chronic period following stroke and correlated with motor outcome. Within our study, the upper tract and partial tract segments showed strong correlations between integrity and motor outcomes (AHA and MA). However, within the fiber tracking method, depending on the portion of the tract analyzed diffusion characteristics were different. The diffusion asymmetries determined from the full tract were consistently different from the other tract portions, with the exception of the upper tract portion. Therefore, although the overall results are generally similar, it appears slightly different neurological information is available from each approach.

4.4 Correlation to Motor Outcome

Overall, most diffusion variables from most tract methods were associated with motor outcome. As the most sensitive and validated measures, associations with AHA and MA are likely the most clinically relevant. Furthermore, the consistency of associations across both outcomes suggests our DTI measures are functionally valid, covering both uni- and bi-manual motor skills relevant to daily living in children.

The particularly strong correlation between upper tract and motor outcome was not expected. This was an interesting finding because the upper portion of fibers consists of everything above the PLIC and would also be included in the full tract. Only the full and upper portions include the ends of the fibers, which are often thought to be unreliable in DTI. These fibers also carry a higher likelihood of running into other crossing fibers in the white matter. One possible factor accounting for the correlation to motor outcome could be that children with larger lesions were excluded from the upper tract analysis due to not having any fibers to analyze.

Our data suggest that our upper and partial tract methodologies may provide the most clinically relevant assessment of CST integrity in perinatal stroke. Our data suggest that it is not the analysis method employed but the portion of the tract analyzed that provides the best measure of integrity related to CST. These findings not only add to the current debate surrounding which analysis method are superior, they provide new insights into which section of the CST provide the most useful diffusion measurements.

4.5 Arterial versus. Venous Stroke

An additional factor that could potentially influence our diffusion measurements and/or their relationship to motor outcome in perinatal stroke is the stroke subtype itself. Although our sample was not adequately powered to explore specific effects of stroke type, several key differences between the two types may have influenced our results. First, arterial stroke (NAIS and APPIS) is typically associated with larger lesions that involve both cortical and subcortical motor systems and occur at term. PVI, on the other hand, are smaller and purely subcortical lesions that are acquired earlier in gestation (prior to 32 weeks). Therefore, it seems likely that both the timing and location of these lesions could influence the subsequent development and

structure of the CST. In future studies, closer comparisons across the subtypes using DTI, other advanced neuroimaging, and transcranial magnetic stimulation (TMS) may provide further insight into CST neurophysiology in perinatal stroke.

4.6 Future Directions: Modulating Developmental Plasticity

Continuing research is providing knowledge of how the brain naturally develops and recovers following focal perinatal brain injury. When it comes to outcome following unilateral motor cortex lesions, it has been known for some time that younger brains tend to have better outcomes than older ones⁸⁹. Investigations into possible mechanisms of age-related plasticity are ongoing. Combinations of animal and human studies using neuroimaging and brain mapping have defined models of plastic reorganization^{90,91} that focus on four primary components: the lesioned and non-lesioned motor cortex, their intra and inter-hemispheric connections with each other and their influence on the spinal motor neuron pools. Within these models, the CST plays an essential role. The ability of DTI to characterize the CST may possibly contribute to a better understanding of both the ipsi- and contra-lesional CST. Establishing motor control in the lesioned hemisphere⁹²⁻⁹⁴ and the persistence of contralateral projections^{95,96} have both been associated with better function. Combining the abilities of DTI (visualization of white matter tracts and quantifying neural fiber composition, integrity and orientation) with other investigations (fMRI and transcranial magnetic stimulation, TMS) will aid to further define models of plastic organization after perinatal stroke.

New therapeutic targets that will advance treatments for children with CP have been identified as a direct result of these models. Using non-invasive brain stimulation like repetitive transcranial magnetic therapy (rTMS) we are able to start implementing the information gathered

from studies. For example, in adult stroke, inhibitory rTMS that was given over the non-lesioned hemisphere improved motor function in the chronic stage after stroke⁹⁷. Studies are currently being developed to use DTI to detect neurophysiological changes, pre and post therapeutic intervention as a measure of plastic change. Therefore, further optimizing CST DTI methods in children with perinatal stroke will add additional potential for the better understanding of motor plasticity in children with CP and aid in generating better therapies in the future.

4.7 Limitations

1. One significant limitation of our study was that we did not have a control population. While we were able to generate SI's for each patient to study integrity, it has been shown recently that mean diffusion variable values are more reliable and sensitive than diffusion asymmetry values⁶⁸. With the addition of a control population we would be able to investigate the mean diffusion values within both the ipsilesional and contralesional CST separately with a healthy population. This would provide a greater degree of information on the extent of the damage.
2. Due to the complexity of obtaining comprehensive testing on all children, only 16 of our subjects had the most robust motor outcomes (AHA and MA). While we were still able to show high correlation to motor outcome, a larger population would provide more power to ask more questions.
3. In the present study only six gradient directions with six repeats were acquired: significantly less than what has been used in some other stroke studies^{46,66-68,82}. However, we do not feel that this significantly compromised the accuracy of our measures as many other studies have employed similar protocols and ours was developed by experts in the field. That being said, there may be benefits associated with increased number of directions, such as improved tensor

calculation for each voxel. More gradient directions may improve the reliability and sensitivity of the DTI analysis. Future studies are now underway using a new 3T MRI DTI protocol so these and other advantages can help advance the work started here.

4. A common and unavoidable issue when using the streamline method for tractography is that the fiber tracking uses a minimum FA threshold as a defining parameter. This prevents tracking of gray matter or CSF which is essential. However, it also ultimately means that the DTI parameter differences we described may be underestimated as possibly not all of the “degraded” tract is being investigated.

5. Lastly, we used a fixed size ROI within the cerebral peduncle when performing the cross-sectional ROI analysis, allowing us to only capture a portion of the diffusion instead of manually drawing around the entire area. However, due to the degree of damage of the tract in some children, we felt that this was the fairest way to assess the area within the cerebral peduncles for our population.

4.8 Conclusions

Our study of CST integrity as measured by diffusion properties using DTI in perinatal stroke supports the following conclusions: 1) DTI is a feasible method for quantifying the diffusion parameters within the CST in the chronic stage following perinatal stroke. 2) Taken as a ratio of lesioned/non-lesioned, symmetry of different diffusion variables varies depending on the portion of the tract measured. 3) Both fiber tracking and cross-sectional ROI analysis approaches can quantify CST integrity in perinatal stroke. 4) FA, RD, and MD show the greatest correlation with long term motor outcomes with RD possibly being the single most clinically relevant measure. 5)

The upper and partial tract methodologies may provide the most clinically relevant assessment of CST integrity in perinatal stroke.

REFERENCES

1. Nelson KB. Perinatal ischemic stroke. *Stroke*. 2007; 38:742-745
2. Mineyko A, Kirton A. The black box of perinatal ischemic stroke pathogenesis. *J Child Neurol*. 2011; 26:1154-1162
3. Sreenan C, Bhargava R, Robertson CM. Cerebral infarction in the term newborn: clinical presentation and long- term outcome. *J Pediatr*. 2000; 137:351-355
4. Raju TN, Nelson KB, Ferriero D et al. Ischemic perinatal stroke: summary of a workshop sponsored by the National Institute of Child Health and Human Development and the National Institute of Neurological Disorders and Stroke. *Pediatrics*. 2007; 120:609-616
5. Devetten G, Coutts SB, Hill MD et al. Acute Corticospinal Tract Wallerian Degeneration Is Associated With Stroke Outcome. *Stroke*. 2010;
6. Kirton A, deVeber G, Pontigon AM et al. Presumed perinatal ischemic stroke: vascular classification predicts outcomes. *Ann Neurol*. 2008; 63:436-443
7. Kirton A, deVeber G. Advances in perinatal ischemic stroke. *Pediatr Neurol*. 2009; 40:205-214
8. Kirton A. Modeling developmental plasticity after perinatal stroke: Defining central therapeutic targets in cerebral palsy. *Pediatric Neurology* . 2012.

Ref Type: Generic

9. Trauner DA, Chase C, Walker P et al. Neurologic profiles of infants and children after perinatal stroke. *Pediatr Neurol*. 1993; 9:383-386
10. Golomb MR, MacGregor DL, Domi T et al. Presumed pre- or perinatal arterial ischemic stroke: risk factors and outcomes. *Ann Neurol*. 2001; 50:163-168
11. Uvebrant P. Hemiplegic cerebral palsy. Aetiology and outcome. *Acta Paediatr Scand Suppl*. 1988; 345:1-100
12. Kirton A, deVeber G. Perinatal ischemic stroke. *Stroke Reviews*. 2006; 10:38-47
13. Wu YW, March WM, Croen LA et al. Perinatal stroke in children with motor impairment: a population-based study. *Pediatrics*. 2004; 114:612-619
14. Govaert P, Matthys E, Zecic A et al. Perinatal cortical infarction within middle cerebral artery trunks. *Arch Dis Child Fetal Neonatal Ed*. 2000; 82:F59-F63
15. de Vries LS, Groenendaal F, Eken P et al. Infarcts in the vascular distribution of the middle cerebral artery in preterm and fullterm infants. *Neuropediatrics*. 1997; 28:88-96
16. Abels L, Lequin M, Govaert P. Sonographic templates of newborn perinatal stroke. *Pediatr Radiol*. 2006; 36:663-669
17. Kirton A, Shroff M, Pontigon AM et al. Risk factors and presentations of periventricular venous infarction vs arterial presumed perinatal ischemic stroke. *Arch Neurol*. 2010; 67:842-848

18. Guyer B, Hoyert DL, Martin JA et al. Annual summary of vital statistics--1998. *Pediatrics*. 1999; 104:1229-1246
19. de Vries LS, Rademaker KJ, Groenendaal F et al. Correlation between neonatal cranial ultrasound, MRI in infancy and neurodevelopmental outcome in infants with a large intraventricular haemorrhage with or without unilateral parenchymal involvement. *Neuropediatrics*. 1998; 29:180-188
20. de Vries LS, Roelants-van Rijn AM, Rademaker KJ et al. Unilateral parenchymal haemorrhagic infarction in the preterm infant. *Eur J Paediatr Neurol*. 2001; 5:139-149
21. Ghi T, Simonazzi G, Perolo A et al. Outcome of antenatally diagnosed intracranial hemorrhage: case series and review of the literature. *Ultrasound Obstet Gynecol*. 2003; 22:121-130
22. Elchalal U, Yagel S, Gomori JM et al. Fetal intracranial hemorrhage (fetal stroke): does grade matter? *Ultrasound Obstet Gynecol*. 2005; 26:233-243
23. Takanashi J, Barkovich AJ, Ferriero DM et al. Widening spectrum of congenital hemiplegia: Periventricular venous infarction in term neonates. *Neurology*. 2003; 61:531-533
24. Takanashi J, Tada H, Barkovich AJ et al. Magnetic resonance imaging confirms periventricular venous infarction in a term-born child with congenital hemiplegia. *Dev Med Child Neurol*. 2005; 47:706-708

25. Cohen ME, Duffner PK. Prognostic indicators in hemiparetic cerebral palsy. *Ann Neurol.* 1981; 9:353-357
26. Humphreys P, Whiting S, Pham B. Hemiparetic cerebral palsy: clinical pattern and imaging in prediction of outcome. *Can J Neurol Sci.* 2000; 27:210-219
27. Niemann G, Wakat JP, Krageloh-Mann I et al. Congenital hemiparesis and periventricular leukomalacia: pathogenetic aspects on magnetic resonance imaging. *Dev Med Child Neurol.* 1994; 36:943-950
28. Wiklund LM, Uvebrant P, Flodmark O. Morphology of cerebral lesions in children with congenital hemiplegia. A study with computed tomography. *Neuroradiology.* 1990; 32:179-186
29. Wu YW, Lindan CE, Henning LH et al. Neuroimaging abnormalities in infants with congenital hemiparesis. *Pediatr Neurol.* 2006; 35:191-196
30. Domi T, deVeber G, Shroff M et al. Corticospinal tract pre-wallerian degeneration: a novel outcome predictor for pediatric stroke on acute MRI. *Stroke.* 2009; 40:780-787
31. Tan M, deVeber G, Shroff M et al. Sagittal sinus compression is associated with neonatal cerebral sinovenous thrombosis. *Pediatrics.* 2011; 128:e429-e435
32. Kirton A, Armstrong-Wells J, Chang T et al. Symptomatic neonatal arterial ischemic stroke: the International Pediatric Stroke Study. *Pediatrics.* 2011; 128:e1402-e1410

33. Kirton A, Wei X. Teaching neuroimages: confirmation of prenatal periventricular venous infarction with susceptibility-weighted MRI. *Neurology*. 2010; 74:e48
34. Lama S, Qiao M, Kirton A et al. Imaging corticospinal degeneration in neonatal rats with unilateral cerebral infarction. *Exp Neurol*. 2011; 228:192-199
35. Tan MA, Miller E, Shroff MM et al. Alleviation of Neonatal Sinovenous Compression to Enhance Neonatal Cerebral Venous Blood Flow. *J Child Neurol*. 2012;
36. Mercuri E, Cowan F, Gupte G et al. Prothrombotic disorders and abnormal neurodevelopmental outcome in infants with neonatal cerebral infarction. *Pediatrics*. 2001; 107:1400-1404
37. Taylor TN, Davis PH, Torner JC et al. Lifetime cost of stroke in the United States. *Stroke*. 1996; 27:1459-1466
38. Lee J, Croen LA, Lindan C et al. Predictors of outcome in perinatal arterial stroke: A population-based study. *Ann Neurol*. 2005; 58:303-308
39. Mercuri E, Jongmans M, Bouza H et al. Congenital hemiplegia in children at school age: assessment of hand function in the non-hemiplegic hand and correlation with MRI. *Neuropediatrics*. 1999; 30:8-13
40. Kitchen L, Westmacott R, Friefeld S et al. The pediatric stroke outcome measure: a validation and reliability study. *Stroke*. 2012; 43:1602-1608

41. Holmefur M, Krumlinde-sundholm L, Eliasson AC. Interrater and intrarater reliability of the Assisting Hand Assessment. *American Journal of Occupational Therapy*. 2007; 61:79-84
42. Krumlinde-sundholm L, Holmefur M, Kottorp A et al. The Assisting Hand Assessment: current evidence of validity, reliability, and responsiveness to change. *Developmental Medicine & Child Neurology*. 2007; 49:259-264
43. Cusick A, Vasquez M, Knowles L et al. Effect of rater training on reliability of Melbourne Assessment of Unilateral Upper Limb Function scores. *Dev Med Child Neurol*. 2005; 47:39-45
44. Greaves S, Imms C, Dodd K et al. Assessing bimanual performance in young children with hemiplegic cerebral palsy: a systematic review. *Dev Med Child Neurol*. 2010; 52:413-421
45. Gilmore R, Sakzewski L, Boyd R. Upper limb activity measures for 5- to 16-year-old children with congenital hemiplegia: a systematic review. *Dev Med Child Neurol*. 2010; 52:14-21
46. Roze E, Harris PA, Ball G et al. Tractography of the corticospinal tracts in infants with focal perinatal injury: comparison with normal controls and to motor development. *Neuroradiology*. 2012; 54:507-516
47. Schaefer PW, Grant PE, Gonzalez RG. Diffusion-weighted MR imaging of the brain. *Radiology*. 2000; 217:331-345

48. Mercuri E, Rutherford M, Cowan F et al. Early prognostic indicators of outcome in infants with neonatal cerebral infarction: a clinical, electroencephalogram, and magnetic resonance imaging study. *Pediatrics*. 1999; 103:39-46
49. Pineiro R, Pendlebury ST, Smith S et al. Relating MRI changes to motor deficit after ischemic stroke by segmentation of functional motor pathways. *Stroke*. 2000; 31:672-679
50. Zhu LL, Lindenberg R, Alexander MP et al. Lesion load of the corticospinal tract predicts motor impairment in chronic stroke. *Stroke*. 2010; 41:910-915
51. Li D, Hodge J, Wei XC et al. Reduced ipsilesional cortical volumes in fetal periventricular venous infarction. *Stroke*. 2012; 43:1404-1407
52. Gauthier LV, Taub E, Mark VW et al. Atrophy of spared gray matter tissue predicts poorer motor recovery and rehabilitation response in chronic stroke. *Stroke*. 2012; 43:453-457
53. Dong Q, Welsh RC, Chenevert TL et al. Clinical applications of diffusion tensor imaging. *J Magn Reson Imaging*. 2004; 19:6-18
54. Nucifora PG, Verma R, Lee SK et al. Diffusion-tensor MR imaging and tractography: exploring brain microstructure and connectivity. *Radiology*. 2007; 245:367-384
55. Yamada K, Sakai K, Akazawa K et al. MR tractography: a review of its clinical applications. *Magn Reson Med Sci*. 2009; 8:165-174

56. Jiang H, van Zijl PC, Kim J et al. DtiStudio: resource program for diffusion tensor computation and fiber bundle tracking. *Comput Methods Programs Biomed.* 2006; 81:106-116
57. Ludeman NA, Berman JI, Wu YW et al. Diffusion tensor imaging of the pyramidal tracts in infants with motor dysfunction. *Neurology.* 2008; 71:1676-1682
58. Glenn OA, Ludeman NA, Berman JI et al. Diffusion tensor MR imaging tractography of the pyramidal tracts correlates with clinical motor function in children with congenital hemiparesis. *AJNR Am J Neuroradiol.* 2007; 28:1796-1802
59. Beaulieu C. The basis of anisotropic water diffusion in the nervous system - a technical review. *NMR Biomed.* 2002; 15:435-455
60. Wakana S, Jiang H, Nagae-Poetscher LM et al. Fiber tract-based atlas of human white matter anatomy. *Radiology.* 2004; 230:77-87
61. Rollins NK. Clinical applications of diffusion tensor imaging and tractography in children. *Pediatr Radiol.* 2007; 37:769-780
62. Wakana S, Caprihan A, Panzenboeck MM et al. Reproducibility of quantitative tractography methods applied to cerebral white matter. *Neuroimage.* 2007; 36:630-644
63. Tournier JD, Mori S, Leemans A. Diffusion tensor imaging and beyond. *Magn Reson Med.* 2011; 65:1532-1556

64. Pierpaoli C, Barnett A, Pajevic S et al. Water diffusion changes in Wallerian degeneration and their dependence on white matter architecture. *Neuroimage*. 2001; 13:1174-1185
65. Mori S, van Zijl PC. Fiber tracking: principles and strategies - a technical review. *NMR Biomed*. 2002; 15:468-480
66. Lindenberg R, Renga V, Zhu LL et al. Structural integrity of corticospinal motor fibers predicts motor impairment in chronic stroke. *Neurology*. 2010; 74:280-287
67. Lindenberg R, Zhu LL, Ruber T et al. Predicting functional motor potential in chronic stroke patients using diffusion tensor imaging. *Hum Brain Mapp*. 2012; 33:1040-1051
68. Borich MR, Wadden KP, Boyd LA. Establishing the reproducibility of two approaches to quantify white matter tract integrity in stroke. *Neuroimage*. 2012; 59:2393-2400
69. Moller M, Frandsen J, Andersen G et al. Dynamic changes in corticospinal tracts after stroke detected by fibretracking. *J Neurol Neurosurg Psychiatry*. 2007; 78:587-592
70. Radlinska B, Ghinani S, Leppert IR et al. Diffusion tensor imaging, permanent pyramidal tract damage, and outcome in subcortical stroke. *Neurology*. 2010; 75:1048-1054
71. Schaechter JD, Fricker ZP, Perdue KL et al. Microstructural status of ipsilesional and contralesional corticospinal tract correlates with motor skill in chronic stroke patients. *Hum Brain Mapp*. 2009; 30:3461-3474

72. Yu C, Zhu C, Zhang Y et al. A longitudinal diffusion tensor imaging study on Wallerian degeneration of corticospinal tract after motor pathway stroke. *Neuroimage*. 2009; 47:451-458
73. Lebel C, Gee M, Camicioli R et al. Diffusion tensor imaging of white matter tract evolution over the lifespan. *Neuroimage*. 2012; 60:340-352
74. Eluvathingal TJ, Hasan KM, Kramer L et al. Quantitative diffusion tensor tractography of association and projection fibers in normally developing children and adolescents. *Cereb Cortex*. 2007; 17:2760-2768
75. Staudt M. (Re-)organization of the developing human brain following periventricular white matter lesions. *Neurosci Biobehav Rev*. 2007; 31:1150-1156
76. Murakami A, Morimoto M, Yamada K et al. Fiber-tracking techniques can predict the degree of neurologic impairment for periventricular leukomalacia. *Pediatrics*. 2008; 122:500-506
77. Yoshida S, Hayakawa K, Yamamoto A et al. Quantitative diffusion tensor tractography of the motor and sensory tract in children with cerebral palsy. *Dev Med Child Neurol*. 2010; 52:935-940
78. Glenn OA, Henry RG, Berman JI et al. DTI-based three-dimensional tractography detects differences in the pyramidal tracts of infants and children with congenital hemiparesis. *J Magn Reson Imaging*. 2003; 18:641-648

79. Heller SL, Heier LA, Watts R et al. Evidence of cerebral reorganization following perinatal stroke demonstrated with fMRI and DTI tractography. Clin Imaging. 2005; 29:283-287
80. Thomalla G, Glauche V, Koch MA et al. Diffusion tensor imaging detects early Wallerian degeneration of the pyramidal tract after ischemic stroke. Neuroimage. 2004; 22:1767-1774
81. Concha, Luis. Diffusion tensor tractography of temporal lobe epilepsy. 2008.
Ref Type: Thesis/Dissertation
82. van der Aa NE, Leemans A, Northington FJ et al. Does diffusion tensor imaging-based tractography at 3 months of age contribute to the prediction of motor outcome after perinatal arterial ischemic stroke? Stroke. 2011; 42:3410-3414
83. Kirton A, Shroff M, Visvanathan T et al. Quantified corticospinal tract diffusion restriction predicts neonatal stroke outcome. Stroke. 2007; 38:974-980
84. Song SK, Sun SW, Ju WK et al. Diffusion tensor imaging detects and differentiates axon and myelin degeneration in mouse optic nerve after retinal ischemia. Neuroimage. 2003; 20:1714-1722
85. Song SK, Sun SW, Ramsbottom MJ et al. Dysmyelination revealed through MRI as increased radial (but unchanged axial) diffusion of water. Neuroimage. 2002; 17:1429-1436

86. Gulani V, Webb AG, Duncan ID et al. Apparent diffusion tensor measurements in myelin-deficient rat spinal cords. *Magn Reson Med*. 2001; 45:191-195
87. Drobyshevsky A, Derrick M, Wyrwicz AM et al. White matter injury correlates with hypertonia in an animal model of cerebral palsy. *J Cereb Blood Flow Metab*. 2007; 27:270-281
88. Tang PF, Ko YH, Luo ZA et al. Tract-specific and region of interest analysis of corticospinal tract integrity in subcortical ischemic stroke: reliability and correlation with motor function of affected lower extremity. *AJNR Am J Neuroradiol*. 2010; 31:1023-1030
89. Kennard MA. Age and other factors in motor recovery from precentral lesions in monkeys. *Am J Physiol*. 1936; 115:137-146
90. Eyre JA. Corticospinal tract development and its plasticity after perinatal injury. *Neurosci Biobehav Rev*. 2007; 31:1136-1149
91. Martin JH, Friel KM, Salimi I et al. Activity- and use-dependent plasticity of the developing corticospinal system. *Neurosci Biobehav Rev*. 2007; 31:1125-1135
92. Werhahn KJ, Conforto AB, Kadom N et al. Contribution of the ipsilateral motor cortex to recovery after chronic stroke. *Ann Neurol*. 2003; 54:464-472
93. Ward NS, Cohen LG. Mechanisms underlying recovery of motor function after stroke. *Arch Neurol*. 2004; 61:1844-1848

94. Rossini PM, Calautti C, Pauri F et al. Post-stroke plastic reorganisation in the adult brain. *Lancet Neurol.* 2003; 2:493-502
95. Kirton A, Chen R, Friefeld S et al. Contralesional repetitive transcranial magnetic stimulation for chronic hemiparesis in subcortical paediatric stroke: a randomised trial. *Lancet Neurol.* 2008; 7:507-513
96. Kirton A, deVeber G, Gunraj C et al. Cortical excitability and interhemispheric inhibition after subcortical pediatric stroke: Plastic organization and effects of rTMS. *Clin Neurophysiol.* 2010;
97. Hsu WY, Cheng CH, Liao KK et al. Effects of repetitive transcranial magnetic stimulation on motor functions in patients with stroke: a meta-analysis. *Stroke.* 2012; 43:1849-1857